ISSN : 0019-5693

INDIAN JOURNAL
OF
THEORETICAL PHYSICS

VOLUME 66 NOS. 1, 2

JANUARY, 2018 — JUNE, 2018

Published by the

CALCUTTA INSTITUTE OF THEORETICAL PHYSICS
(Formerly, INSTITUTE OF THEORETICAL PHYSICS)
"BIGNAN KUTIR"
4/1, MOHAN BAGAN LANE, KOLKATA-700 004

(UGC approved and refereed Journal)

ISSN : 0019-5693

INDIAN JOURNAL
OF
THEORETICAL PHYSICS

[Founder President : Late Prof. K. C. Kar, D.Sc.]

VOLUME 66 **NOS. 1, 2**

JANUARY, 2018 — JUNE, 2018

Co-Published by the

WILCOX BOOKS & PERIODICALS CO.

8/2/A, Neogipara Road, Kolkata – 700 036

BLANK

INDIAN JOURNAL
OF
THEORETICAL PHYSICS

"BIGNAN KUTIR"
4/1, MOHAN BAGAN LANE, KOLKATA-700 004, INDIA

SUBSCRIPTION RATE

INDIA : (For Library & Institute)
₹ 1500.00 for Vol. 64, 2016 and onwards
FOREIGN : $ 350 for Vol. 64, 2016 and onwards
Drafts, Orders, Enquiries & Claim for Non-Receipt of Journal should be sent to :

WILCOX BOOKS & PERIODICALS CO.
8/2/A, NEOGIPARA ROAD
KOLKATA – 700 036 (INDIA)
Website : www.wilcoxjournals.com
E-mail : wilcoxbooks@yahoo.com
: wilcoxbooks@gmail.com
Phone : 91-3325771147
Mobile : 91-9231675520

BLANK

C O N T E N T S

BLANK

INDIAN JOURNAL OF THEORETICAL PHYSICS, VOL. 66, NOS. 1 & 2, 2018

On the determination of activation energy of thermoluminescence peaks recorded under hyperbolic heating scheme and obeying mixed order kinetics

Ananda Sarkar
Department of Physics, Acharya Prafulla Chandra College
New Barrackpore, Kolkata - 700131, India
E-mail : ananda@apccollege.ac.in

[**Abstract:** In the present work we present a set of expressions for the determination of activation energy of thermoluminescence (*TL*) peaks recorded under hyperbolic heating scheme and obeying mixed order kinetics. The suitability of present set of expressions has been tested by applying them to a number of computer generated and experimental *TL* peaks and encouraging results have been obtained.]

Keywords: Thermoluminescence; Hyperbolic heating scheme; Activation energy; Mixed-order kinetics

1. Introduction

Thermoluminescence (*TL*) is the emission of light by a semiconducting or insulating material on heating after previous exposure to ionizing radiations such as *X*-rays, γ-rays etc. The phenomenon has important applications in the fields of dating, dosimetry and spectroscopic studies of trapping levels[1,2]. The most popular model of *TL* is kinetic order model (*KOM*)[1,2] in which the *TL* process can be explained in terms of three parameters namely activation energy (E), order of kinetics (b) and frequency factor (s). This model in the limit $b \to 1$ includes the first order kinetics model (*FOKM*) of Randal and Wilikils[3]. For $b = 2$, the model reduces the second order kinetics model (*SOKM*) of Garlick and Gibson[4]. But the main drawback of *KOM* is that in it there is no provision for the inclusion of thermally disconnected deep traps (*TDDT*). The importance of *TDDT*'s in

an overall model of *TL* has been discussed by Fain et al[5,6]. In mixed order kinetics model (*MOKM*) the effect of *TDDT*'s has been taken into account. Chen et al[7] and Kittis et al[8] have carried out elaborate investigations on *TL* process under *MOKM* formalism. But all the above mentioned works have been carried out for *TL* recorded under linear heating sceme (*LHS*). We know that hyperbolic heating scheme (*HHS*) is an important adjunct[9-13] to *LHS*. In the present paper we plan to investigate *TL* recorded under *HHS* in the *MOKM* formalism. We attempt to present a set of expressions for the evaluation of activation energy of *TL* peaks recorded under *HHS*. The suitability of these expressions has been assessed by considering both the computer generated and experimental *TL* peaks recorded under *HHS*. To the best of our knowledge till date there is no work on *MOKM* in *TL* recorded under hyperbolic heating profile.

2. Methodology

In *MOKM* the expression for *TL* intensity $I(T)$ at temperature T is given by[7]

$$I(T) = -\frac{dn}{dt} = s'n(n+c)\exp\left(-\frac{E}{kT}\right) \quad \ldots \quad (1)$$

with $s' = \frac{sA_m}{NA_n}$ … (2)

where s is the frequency factor, n is the concentration of trapped electrons at time t, c is the concentration of *TDDT*'s, E is the activation energy, k is the Boltzmann constant , N is the concentration of active electron traps, A_m and A_n are respectively the retrapping and recombination co-efficient in units of $cm^3 sec^{-1}$. The hyperbolic heating profile is given by[9-13]

$$\frac{1}{T} = \frac{1}{T_0} - \beta' t \quad \ldots \quad (3)$$

where T_0 is the temperature at time $t = 0$, T is the temperature at time t and β' is a constant. From equation (3) one can write

$$\frac{dT}{dt} = \beta' T^2 \quad \ldots \quad (4)$$

Using equations (1) and (4) the *TL* intensity $I(T)$ at absolute temperature in *MOKM* for *HHS* is given by

$$I(T) = \frac{\alpha c^2 s' \exp\left[\gamma\left(e^{-u} - e^{-u_0}\right)\right]\exp(-u)}{\left[\exp\left\{\gamma\left(e^{-u} - e^{-u_0}\right) - \alpha\right\}\right]^2} \quad \ldots \quad (5)$$

with

$$\alpha = n_0/(n_0 + c) \quad \ldots \quad (6)$$

$$\gamma = \frac{cs'k}{\beta' E} \quad \ldots \quad (7)$$

$$u = E/kT \quad \ldots \quad (8)$$

$$u_0 = E/kT_0 \quad \ldots \quad (9)$$

n_0 is the initial concentration of trapped electrons.

The condition for maximum intensity (I_m) can be expressed as

$$[\alpha + \exp\{\gamma(e^{-u_m} - e^{-u_0})\}]\,(1 - \gamma e^{u_m} - 2\alpha) = 0 \quad \ldots \quad (10)$$

The temperature T_m corresponding to the maximum intensity I_m can be found by solving equation (10) by Newton Raphson method[14].

Knowing T_m we can find out peak intensity $I(T_m)$ by using equation (5).

The fractional intensity (x) at temperature T is given by

$$x = \frac{I}{I_m} = B\exp(u_m - u)\frac{\exp\left[\gamma\left(e^{-u} - e^{-u_0}\right)\right]}{[\exp\{\gamma\left(e^{-u_m} - e^{-u_0}\right)\}]^2} \quad \ldots \quad (11)$$

where $B = \dfrac{[\exp\{\gamma\left(e^{-u_m} - e^{-u_0}\right) - \alpha\}]^2}{\exp\left[\gamma\left(e^{-u} - e^{-u_0}\right) - \alpha\right]}$ … (12)

and $u_m = \dfrac{E}{kT_m}$

Again by solving equation (11) by Newton Raphson method for fractional intensity $x = \frac{1}{2}$ one can evaluate

$$u_1 = \frac{E}{kT_1} \text{ and } u_2 = \frac{E}{kT_2} \quad \ldots \quad (13)$$

where T_1 and T_2 are respectively the temperatures corresponding to half intensity points in the rising and falling sides of the *TL* peak.

By using the technique of non linear regression[15] it has been found that for a an arbitrary value of x, say $x = \frac{1}{2}$ it is possible to write

$$u_1 - u_m = A_\tau^{(0)} + A_\tau^{(1)}\mu_g + A_\tau^{(2)}\mu_g^2 \quad \ldots \quad (14)$$

$$u_m - u_2 -= A_\delta^{(0)} + A_\delta^{(1)}\mu_g + A_\delta^{(2)}\mu_g^2 \quad \ldots \quad (15)$$

$$u_1 - u_2 = A_\omega^{(0)} + A_\omega^{(1)}\mu_g + A_\omega^{(2)}\mu_g^2 \quad \ldots \quad (16)$$

and symmetry factor μ_g is given by[13]

$$\mu_g(x) = \frac{u_m - u_2}{u_1 - u_2} \quad \ldots \quad (17)$$

where $A_j^{(i)}$ $(i = 0,1,2,\ j = \tau, \delta, \omega)$ are the regression coefficients.

It is to be noted that following Chen and Kirsh[17] $\tau = (T_m - T_1)$, $\delta = (T_2 - T_m)$ are respectively rising and falling sides half widths of the *TL* peak corresponding to the fractional intensity $x = \frac{1}{2}$ and $\omega = (T_2 - T_1)$ is the full width of the peak at $x = \frac{1}{2}$.

By using equations (13) and (14), equations (15)-(17) can be expressed as

$$E_\tau = \frac{kT_mT_1}{\tau}(A_\tau^{(0)} + A_\tau^{(1)}\mu_g + A_\tau^{(2)}\mu_g^2) \quad \ldots \quad (18)$$

$$E_\delta = \frac{kT_mT_2}{\delta}(A_\delta^{(0)} + A_\delta^{(1)}\mu_g + A_\delta^{(2)}\mu_g^2) \quad \ldots \quad (19)$$

$$E_\omega = \frac{kT_2.T_1}{\omega}(A_\omega^{(0)} + A_\omega^{(1)}\mu_g + A_\omega^{(2)}\mu_g^2) \quad \ldots \quad (20)$$

3. Results and discussions

In Table 1 we present the coefficients $A_j^{(i)}$ for different values of *i* and *j*. Mixed order *TL* peaks have generated with $E = 1\ eV$, $n_0 = N = 10^{10}\ cm^{-3}$, $A_m = A_n = 10^{-7}\ cm^3\ sec^{-1}$, $\beta' = 6.78 \times 10^{-6}\ K^{-1} sec^{-1}$ and s= $10^{12} sec^{-1}$ for different values of α ranging from 0.1 to 0.9.

Table 1

Coefficients $A_j^{(i)}$ $(i = 0,1,2)$ occurring in equations (19)-(21).

J	$A_j^{(0)}$	$A_j^{(1)}$	$A_j^{(2)}$
τ	1.0174	0.5064	3.9938
δ	2.5036	-13.1903	23.4059
ω	3.1566	-13.6505	27.3196

We have calculated the activation energy of the peaks by using the expressions of activation energies (equations (19)-(21)). The results are presented in Table 2.

Table 2

Activation energies E_j $(j = \tau, \delta, \omega)$ of some computer generated *MOKM TL* peaks for $E_{in} = 1.0\ eV$, $s = 10^{12} sec^{-1}$, $A_m = A_n = 10^{-7} cm^3 sec^{-1}$, $N = n_0 = 10^{12} cm^{-3}$, $\beta' = 6.76 \times 10^{-6} K^{-1} sec^{-1}$ using present set of expressions (equations (17)-(19)) corresponding different values of α.

α	$E_\tau\ (eV)$	$E_\delta (eV)$	$E_\omega\ (eV)$
0.1	1.0000	1.0002	1.0005
0.2	1.0000	0.9994	1.0000
0.3	1.0	0.9993	0.9999
0.4	1.0	0.9995	0.9994
0.5	1.0	1.0	1.0
0.6	1.0	1.0	1.0
0.7	1.0	1.0006	1.0002
0.8	1.0	1.0005	1.0
0.9	0.9999	0.9999	0.9997

It is evident from Table 2 that the values of E_τ, E_δ and E_ω are good agreement with the input value of $E = E_{in}$.

We have also calculated μ_g for different values of α and using the technique of non linear regression[15] $\mu_g(0.5)$ can be expressed as a quadratic function of α given by

$$\mu_g(0.5) = 0.4042 + 0.08726\alpha + 0.00711\alpha^2 \quad \ldots \quad (21)$$

If $\mu_g(0.5)$ is known then by using equation (20) α which is an important parameter in *MOKM* can be found out. The curve connecting $\mu_g(0.5)$ and α is presented in Figure 1. We see that μ_g increases with α.

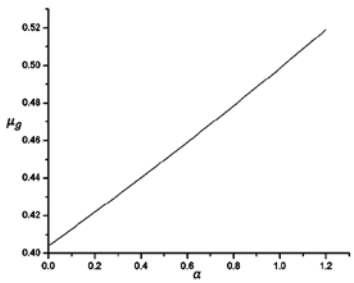

Figure 1

Variation of μ_g with α.

Finally the applicability of the present set of expressions for the determination of activation energy is studied by considering 445*K* peak of Al_2O_3 (Figure 2) irradiated with *X*-rays and recorded under hyperbolic heating scheme[17] with $\beta' = 1.3 \times 10^{-6} K^{-1} sec^{-1}$. The peak is fitted by using *MOKM*.

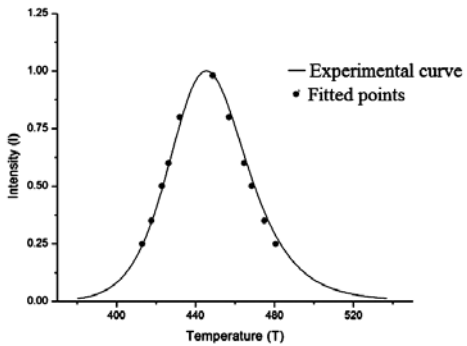

Figure 2

Experimental *TL* peak of *X*-irradiated Al_2O_3.

The fitted parameters are presented in Table 3. The figure of merit[18] value of 0.82% indicates a good fit.

Table 3

Fitted parameters of 445*K TL* peak of Al_2O_3 recorded under hyperbolic heating profile with $\beta' = 1.3 \times 10^{-6}\ K^{-1}sec^{-1}$.

E_{cf} (eV)	s (sec^{-1})	n_0 (cm^{-3})	c (cm^{-3})	α	*FOM* (%)	A_m (cm^3sec^{-1})	A_n (cm^3sec^{-1})
1.30	1.0×10^{13}	1.0×10^{11}	4.71×10^{9}	0.95	0.82	10^{-7}	10^{-7}

In Table 4 we have presented the values of activation energies E_τ, E_δ and E_ω as calculated by using the preset sets of expressions for the 445*K TL* peaks of Al_2O_3 recorded under hyperbolic heating scheme. From Tables 3 and 4 we infer that the values of activation energies as calculated by the present method are in good agreement with the fitted value of *E*. The value of mixed order parameter α as calculated by using equation (20) for μ_g is also presented in Table 4 and it is also in good agreement with the fitted value of α.

Table 4

Activation energies of 445*K TL* peak of Al_2O_3 using equations (17)-(19) and *MOKM* parameter α.

x	$E_\tau\ (eV)$	$E_\delta\ (eV)$	$E_\omega\ (eV)$	α
0.5	1.29	1.28	1.29	0.96

4. Conclusions

In the present work we have reported a set of expressions for the calculation of activation energies of *MOKM TL* peaks recorded under hyperbolic heating scheme. The present set of expressions has been used to calculate the activation energy of some computer generated peaks and calculated values of activation energies for aforesaid peaks show good agreement with the corresponding input values. The present set of expressions has also been used to evaluate the activation energy of 445*K TL*

peak of Al_2O_3 irradiated with *X*-rays. There is fair agreement of the calculated values of activation energies E_τ, E_δ E_ω and E_{cf}. The present finding suggests that the present method can be used for the determination of ctivation energy and *MOKM* parameter α for *MOKM TL* peaks under hyperbolic heating scheme.

References

1. Mckeevar, S. W. S. – "Thermoluminescence of solids", Cambridge University Press, Cambridge (1985).
2. Chen, R. and Pagonis, V. – "Thermally and optically stimulated luminescence: A simulation approach, John Wiley, West Sussex, UK (2011).
3. Randal, J. T. and Wilkins, M. H. T. – Proc. Roy. Soc., London, A, **184**, 366 (1945).
4. Garlick, G. F. J. and Gibson, A. F. – Proc. Phys. Soc., **A60**, 574 (1948).
5. Fain, J., Sanzelle, S., Miallier, D., Montret, M. and Pilleyre, Th. – Radiat. Meas., **23**, 287 (1994).
6. Fain, J., Sanzelle, S., Pilleyre, Th., Miallier, D. and Montret, M. – Radiat. Meas., **30**, 487 (1999).
7. Chen, R., Kristianpoller, N., Davidson, Z. and Visocekas, R. – J. Lumin., **23**, 293 (1981)
8. Kitis, G., Chen, R. and Pagonis, V. – Phys. Stat. Sol., **205**, 1181 (2008).
9. Stamers, K, – J. Phys. E: Sci. Instrum., **12**, 637 (1979).
10. Colvin, G. G., Worpe, E. A. and Gilboy, W. B. – J. Phs. E: Sci. Instrum., **17**, 19 (1984).
11. Kelly, P. J. and Laubitz, M. J. – Can. J. Phys., **45**, 311 (1967).
12. Arnold, W. and Sherwood, H. – J. Phys. Chem., **63**, 2 (1959).
13. Christodoulides, C. – J. Phys., D, **18**, 1555 (1986).
14. Sanyal, D. C. and Das, K. – Introduction to Numerical Analysis", U. N. Dhar and Sons, Kolkata, India (2012).
15. Spiegel, M. R. and Stephen, L. J. – "Theory and Problems in Statistics", 3rd Edn., TMG, New Delhi, India (2000).
16. Chen, R. and Kirsh, Y. – "Analysis of Thermally Stimulated Processes", Pergamon Press, Oxford (1981).
17. Ziniker, W. M., Rusin J. M. and Stoebe, T. G. – J. Mater. Sc., **8**, 407 (1973).
18. Pagonis, V., Kitis, G. and Furetta, C. – "Numerical and Practical Exercises in thermoluminescence", Spinger, New York, (2006).

INDIAN JOURNAL OF THEORETICAL PHYSICS, VOL. 66, NOS. 1 & 2, 2018

Analytical study of diffusivity and shear viscosity of liquid semiconductor

Lalit Kumar Mishra, Gyanesh
University Department of Electronics, B.R.A. Bihar University,
Muzaffarpur-842001, Bihar, India

and

Tarun Kumar Dey
Post Graduate Department of Physics, L.S. College,
Muzaffarpur -842001, Bihar, India
E-mail: tkdeyphy@gmail.com

[**Abstract** : The effective pair potential of liquid semiconductor *Se* is extracted from its experimental structure factor data using an accurate liquid state theory and this shows important basic features. A model potential incorporating the basic features of the structure factor extracted potential is suggested. This model potential is then used to describe through low-order perturbation theory, the structure and related transport properties like self-diffusion coefficient and shear viscosity of this complex liquid over a wide range of temperatures.]

Keywords : Effective pair potential, semiconductor liquid, transport properties

1. Introduction

The crystalline structure of *Se* is made by stacking helical chains and results from a Peierls distortion of a simple cubic structure[1]. The atomic and electronic structures of liquid *Se* at high pressure and high temperature are still not fully understood. The theoretical understanding of the process is hindered by the bonding properties of *Se*[2]. The bonds within the chains are covalent with an energy »2 *eV*/atom whereas the bonds between chains are an order of magnitude smaller but long-range dispersion forces are not negligible and must be taken into account. From the measurement of shear viscosity the melting point an average chain length of 10^4 - 10^5 atoms can be estimated but this number drastically decreases with the increase of

temperature and pressure[3]. The effective pair potential must be complex and liquid-state statistical mechanical calculation appears to be quite puzzling. The complexity of the average intermolecular interaction is reflected in the liquid structure factor of *Se* which is very different from that of simple liquid metals in as much as the first diffraction peak is considerably reduced in magnitude compared to second one as a consequence of it oscillations. This oscillation implies that a considerable fraction of the ring or chain structure found in crystalline structure remains in the liquid state. The structure factors of solid amorphous (*a*-) and liquid (*l*-) *Se* are quite similar. The structural features are likely to be exhibited in the effective pair potential of *Se*. With this view in mind we have extracted effective pair potential of *Se* in liquid state from its *x*-ray structure factor data[4] using an accurate liquid-state theory (the modified hypernetted chain (*MHNC*) method)[5]. The diffraction data is due to Waseda et al[4] and presented in tabulated form.

2. Theoretical model

We propose an approximate model potential for liquid *Se* consistent with the basic features of its structure. The atoms in the chains are strongly bound whereas the interaction between the chains is weak van der Waals type. The application of hydrostatic pressure promotes transfer of electrons from the intra-chain bonding orbitals to bonding states between chains and can bring about a change in the relative charge distribution between inter-chain and intra-chain bonds[6]. We therefore propose a model potential comprising Mie *m*, *n* (*m* = 6 and *n* = 12) potential in conjunction with a repulsive term. The repulsive term is suggested corresponding to empty-core pseudo potential in Thomas Fermi screening approximation[7] to account for the ionic behavior. Thus,

$$\phi(r) = a(r_0/r)^n - b(r_0/r)^m + (z_s^e e^2/r)\cosh^2(kr_c)\exp(-kr), \qquad \ldots \quad (1)$$

where a, b, r_0, z_s, k and r_c are the constants obtained through structure factor data fit and listed in Table 1. We have also obtained the first and second nearest numbers and correspondences distances and are tabulated in Table 2 along with experimental data[4]. The basic features agree approximately with the one extracted from the experimental structure factor data.

For structure factor calculation in low-order perturbation theory, we use the *WCA* separation[8] of the potential into short-range reference term, $\phi_{ref}(r)$ and long-range perturbation term, $\phi_1(r)$

$$\phi_{ref}(r) = \phi(r) - \phi_{min} \quad \text{for } r < r_0$$
$$= 0 \quad \text{for } r > r_0$$

and

$$\phi_1(r) = \phi_{min} \quad \text{for } r < r_0$$
$$= \phi(r) \quad \text{for } r > r_0 \qquad \ldots \quad (2)$$

Table 1

Potential parameters (temp. = 250˚*C*).

a (*a.u.*)	0.052
b (*a.u.*)	0.155
r_0 (*a.u.*)	4.2155
Zs	1.68
k ($a.u.^{i1}$)	0.605
rc (*a.u.*)	1.36

Table 2

	l-Se (250^oC)		
	Present	Experimental	*a-Se*
σ (Å)	3.104	-	-
η	0.47	-	-
r_1 (Å)	2.38	2.36	2.34
n_1	2.29	2.36	2.00
r_2 (Å)	3.36	3.76	3.75
n_2	7.51	6.80	6.40

The structure factor calculation is made for short-range reference part by Jacobs Anderson (*JA*) method and long-range perturbation part contribution obtained in *RPA*[8].

3. Diffusivity

The statistical theory of liquids applies for computation of transport properties like diffusivity witn the help of effective pair and structure factor data[4]. As it is well-known that the soft-part of the intermolecular potential has a dominant role in determining the magnitude of the diffusivity.The positive barrier of the Se potential would have significant role to play in the nature of the self-diffusion co-efficient. We have computed the self-difusion coefficient *D* of *l-Se* based on Helfand-Rice-Nachtrieb (*HRN*) prescription [9,10] given by

$$D = k_B T=(\xi^H + \xi^S + \xi^{SH}); \quad \ldots \quad (3)$$

where ξ^H, ξ^S and ξ^{SH} are the friction constants due to repulsive hard core inter-action, soft interaction between the neighboring atoms and cross effect between the repulsive core and the soft long forces respectively. Explicit expressions could be found elsewhere[4]. In a liquid where diffusion takes place, the motion of a given atom is impeded by its neighbors and several atoms must be moved in order for diffusion to take place. This fact can be taken into account in an *ad hoc* way by allowing atomic mass to be larger than the actual mass. Because of the very nature of the repulsive barrier we hope that this caging effect[11] must be more appropriate for system like *l-Se* and that the atomic mass *m* is to be replaced by an erective larger mass *m**. The effective mass for diffusion includes the mass of the atom itself plus the mass of the neighboring atoms that have to be moved in order for diffusion to take place. Thus the idea of correlation length *l** arises and this is given by the distance over which some rearrangement takes place to accommodate the movement of one atom. The relation between *l** and *m** is such that a volume of dimension *l** contains a number of atoms equal to *m**/*m* and considering hard sphere particles expression is given by

$$m^* = m\eta\, g(\sigma)(l^*=\sigma)^3; \quad \ldots \quad (4)$$

where $g\left(\frac{3}{4}\right)$ is the *PDF* at contact and other terms are as already defined. Like number average chain length[12], we assume $l^*=\frac{3}{4}$ to fall exponentially

with temperature. The value at $250^{\circ}C$ and its fall are determined by fitting the self-diffusion coefficient data at $250^{\circ}C$ and its rate of increase at $250^{\circ}C$ with temperature as available in the literature. The calculated self-diffusion coefficient as a function of temperature is shown in figure 1 along with simulation data[13] and estimation from quasi-elastic neutron scattering (*QENS*) data[14] wherever available. Unfortunately there is no direct experimental measurement of self-diffusion coefficient of *l-Se* available in the literature. The friction constants are also shown which indicate the relative contributions of short-range and long-range interactions.

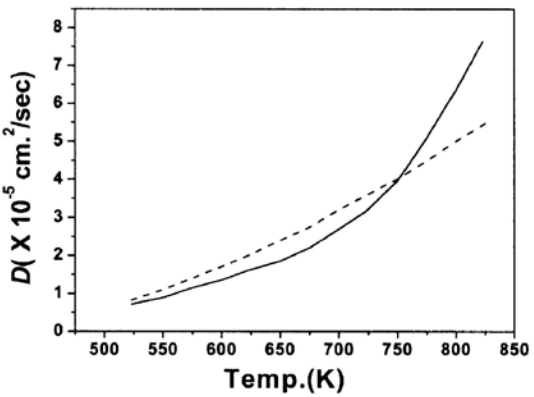

Figure 1

Self diffusion coeffcient vs. temperature. Calculated: (-), simulation/*QENS*: (- - -).

4. Shear viscosity

The shear viscosity is another important macroscopic dynamical property in which *l-Se* has its distinction from other liquids and liquid metals. Near the melting point it is extremely large but drastically reduces with increase of temperature. The number average chain length in *l-Se* is derived from observed shear viscosity data[12]. Eyring developed a theory for rate process which gives a connection between self-diffusion (D) and shear viscosity (μ) coeffcients for dense liquids[11]. This relationship has been often used to estimate the self-diffusion coeffcient from shear viscosity data[14]. The desired relationship is[11]

$$\mu = k_B T a^2 p / D, \qquad \ldots \quad (5a)$$

where a is the spacing between atoms and $\frac{1}{2}$ is the position-dependent

number density. Approximating a by the correlation length and $\frac{1}{2}$ by the *RDF* at contact value we have the shear viscosity formula given by

$$\mu = k_B T l^{*2} p_0 g(\sigma)/D \qquad \ldots (5b)$$

$\frac{1}{20}$ being the atomic number density. The latter approximation is done similar to the one done for effective mass calculation[11]. Using calculated D's we have evaluated from Eq. (5*b*) and the results are shown in figure 2 as a function of temperature. It is indeed surprising to note that Eyring's rate theory results agree so well with observed shear viscosity data.

5. Results and discussion

It is gratifying to note that like *a-Se*, it is possible to conceive of a model effective pair potential for *l-Se*. The characteristic features of the effective pair potential extracted from experimental structure factor data agree generally with the model potential. The model potential parameters listed in Table 1 appear quite reasonable when compared with those of *a-Se*. The hard-core parameters, however, decrease monotonically with increase of temperature (figure 1). The model *RDF* and atomic distribution function $N(r)$ at $250^{\pm}C$ are shown in figure 1 where the temperature effect includes.

In figure 1 the results depicted for self-diffusion coefficient indeed agree well with the data from quasi-elastic neutron scattering (*QENS*) data and also simulation data[13,14] wherever available. The directly measured data for *l-Se* are not available in the literature. The calculated values at higher temperatures appear to be somewhat large but these values agree reasonably with simulation results[13].

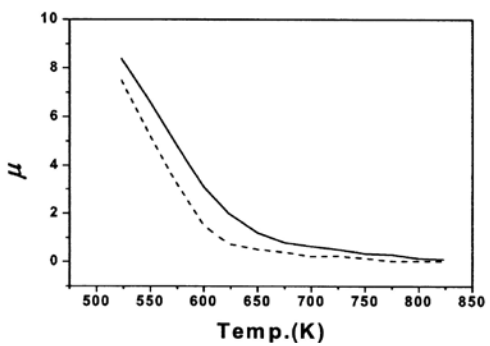

Figure 2

Shear viscosity vs. temperature. Calculated: (…), experimental: (- - -).

In figure 2, we show the results for shear viscosity calculated through Eq. (5*b*). The directly measured data on the shear viscosity are available in the literature and the values are shown for comparison. It is evident that Eyring's rate theory expression with the consideration of effective mass due to caging effect yields viscosity results quite well. The large and rapid decrease in the viscosity with rise of temperature is well-produced by this formula involving self-diffusion constant. The agreement also supports the calculated values of self-diffusion coefficient through Eq. (3).

References

1. Gaspard, J. P., Pellegatti, A., Marinelli, F. and Bichara, C. – Philos. Mag., **B77**, 727 (1998).
2. Bichara, C., Raty, J.Y. and Gaspard, J. P. – J. Non-Cryst. Solids **419,** 250-252, (1999).
3. Perron, J. C., Rabit, J. and Rialland, J. F. – Philos. Mag. **B46**, 321 (1982).
4. Jr. Warren and Dupee, R. – Phys. Rev., **B22**, 2257 (1980).
5. Waseda, Y., Yokoyama, K. and Suzuki, K. – Phys. Condensed Matter, **18**, 293 6(1974). Waseda, Y. – The structure of non-crystalline materials, McGraw-Hill, NY, (1980).
6. Rosenfeld, Y. and Ashcroft, N. W. – Phys. Rev., **A20**, 1208 (1979).
7. Khetrapal, M., Bhandari, D. and Saxena, N.S. – The physics of disordered materials edited by Saxena M.P., Saxena N. S. and Bhandari D., NISCOM, New Delhi, (1997).
8. Martin, R.M., Lucovsky, G. and Haliwell, H. – Phys. Rev., **B13**, 1383 (1976).
9. Hafner, J. and Heine, V. – J. Phys., **F13**, 2479 (1983).
10. Mclaughlin, I. L. and Young, W. H. – J. Phys., **F12**, 245 (1982).
11. Egelstaff, P. A. – An introduction to the liquid state, Clarendon Press, Oxford, (1994).
12. Harrison, D. E. – J. Chem. Phys., **41**, 844 (1964).
13. Almarza, N.G., Enciso, E. and Bermejo, F. J. – Europhys. Lett., **17**, 595 (1992). Caprion, D. and Schobe r H. R. – Phys. Rev., **B62**, 3709 (2000).
14. Kirchhoff, F., Gillan, M. J. and Hollender, J. M. – J. Non-Cryst. Solids, **207**, 924 (1996).
15. Axmann, A., Gissler, W., Kollmar, A. and Springer, T. – Discuss. Faraday Soc., **50**, 74 (1970).

INDIAN JOURNAL OF THEORETICAL PHYSICS, VOL. 66, NOS. 1 & 2, 2018

Causality analysis between solar irradiance and Forbush decrease indices

Sankar Narayan
Department of Instrumentation Science, Jadavpur University,
188, Raja S.C. Mallick Road, Kolkata-700032, India
E-mail: sankar.journal@gmail.com

Amrita Prasad
Department of Mechanical Engineering, Jadavpur University,
188, Raja S.C. Mallick Road, Kolkata-700032, India
E-mail: prasad.amrita1@gmail.com

Soumya Roy
Department of Mechanical Engineering, Jadavpur University,
188, Raja S.C. Mallick Road, Kolkata-700032, India
E-mail: soumyaroy.burdwan@gmail.com

Gautam Bhattacharya
Department of Physics, University Institute of Technology,
University of Burdwan, Golapbag (North), Burdwan-713104, India
E-mail:gautamuit@gmail.com

Subhash Chandra Panja
Department of Mechanical Engineering, Jadavpur University,
188, Raja S.C. Mallick Road, Kolkata-700032, India
E-mail: panja12@gmail.com

and

Koushik Ghosh
Department of Mathematics, University Institute of Technology,
University of Burdwan, Golapbag (North), Burdwan-713104, India
E-mail: koushikg123@yahoo.co.uk

[Abstract: In the present paper we have tried to investigate whether there is any statistical association between solar irradiance and Forbush decrease and if yes whether there is any directionality in this association. The present investigation physically helps us

to understand whether there is any relation between solar-terrestrial climate and cosmic ray intensity. For the present investigation we have taken into account Granger causality analysis and the present study indicates a possible influence of solar irradiance on Forbush decrease.]

Keywords : Total solar irradiance, Forbush decrease, nonlinear phase filter, Granger causality.

1. Introduction

Solar irradiance is measured by the amount of electromagnetic energy plummeted on the surface perpendicular to the incoming radiation at the top of the Earth‘s atmosphere. Total solar irradiance (*TSI*) is the total energy flux over the whole spectrum disembarking at the top of the atmosphere at the mean Sun Earth distance. However, variations in *TSI* might be caused due to the solar phenomena like solar oscillations, granulation, Sunspots, faculae and solar cycle.

Solar luminosity has been found to achieve a maximum value at the very instant at which Sunspot activity is highest during the 11-year Sunspot cycle. The presence of large groups of Sunspots on the Sun's surface produces dips ranging in amplitude from 0.1-0.25% of the solar constant. This reduction in the total solar irradiance has been attributed both to the presence of these Sunspots and to the temporary storage of solar energy over times longer than the Sunspot’s lifetime. When Sunspots explode, they often hurl massive clouds of hot gas away from the Sun. These clouds, called coronal mass ejections (*CME*), contain not only gas but also magnetic force fields, knots of magnetism ripped away from the Sun by the explosion. Magnetic fields deflect charged particles, so when a *CME* sweeps past Earth, it also sweeps away many of the electrically-charged cosmic rays that would otherwise strike our planet. This phenomenon is known as "Forbush decrease" [1]. Forbush decreases (*FDs*) are transient and rapid decreases of the cosmic ray intensity; the decreases are followed by a slow recovery. Though *FDs* are believed to be produced by perturbations in the interplanetary conditions, none of the theories[2,3,4,5] proposed so far to explain *FDs*, has succeeded to completely explain the details of this phenomenon. Scientists investigated one of the most famous *FDs* in galactic cosmic-ray intensity, which occurred on June 8, (1969) close to the Sunspot

maximum of solar cycle 20. The event is well known for its abnormally slow recovery after the maximum intensity depression. The recovery from the decrease in this event took as long as several months even in high-energy region covered by the ground based neutron monitors, while it takes less than a week in most of usual events. Shah et al.[6] reported experimental evidence of recording a major *FD* as a result of the extremely high activity in the Sun and in the heliosphere that took place in October-November (2003) during the declining phase of the 23rd solar cycle. Ifedili[7,8,9] studied a two-step *FD*-type, with large cosmic ray intensity decreases during 13–15 January (1967), 3–5 January (1978), 30 January (1978), 27–28 August (1978), 29–30 September (1978), 24–26 April (1979), 28–29 November (1989), and 29–30 December (1989), each of which appears to be produced by the structure within the shock and sheath preceding. Subramanian et al.[10] measured the ratio of energy density in the turbulent magnetic fields to that in the mean magnetic fields near the *CME* fronts and it was found to be ~2% for the April 11, (2001) *FD* event, ~6% for the November 20, (2003) *FD* event and ~24% for the much more energetic event of October 29, (2003).

There has been a long-lasting debate about the possible connection between cosmic rays and solar-terrestrial climate. Solar cycles and trends are identified as significant components of natural climate variability[11,12]. So any association of *FD* which appears as a direct consequence of decrease in cosmic ray intensity with any measure of solar activity *e.g. TSI* may in turn favour the connection between cosmic ray and solar-terrestrial climate. Laken et al.[13] claimed that during *FD* events both solar irradiance and galactic cosmic ray flux exhibit connected changes. Dragić et al.[14] showed that possibly there is a genuine correlation between the cosmic-ray intensity and the diurnal temperature range. On the other hand, Erlykin and Wolfendale[15] claimed that the effects of cosmic ray on the Earth's atmosphere are very small; it effects in stratosphere but it makes no such significant change at the lower atmosphere, changes in which are the contemporary concerns. In this context we can report that the observed periods of the *TSI* data at 752 days by Rayleigh power spectrum analysis[16], at 740 days by Scargle method of Periodogram[17] and at around 729 days by

FFT[18] are interestingly similar with the periods at 735, 741 and 767 days for *FDI* by Scargle method of Periodogram[19]. Again the observed period of *TSI* at around 1980 days by *FFT*[18] is appreciably similar to the obtained period of the *FDI* at 5-6 years by discrete wavelet transform[20]. This again fuels the possibility of some form of statistical association between solar irradiance and *FD*. In this paper, we have tried to analyze this interaction patterns among *TSI* and *FD*. A question of interest is the evaluation of information flow between these two phenomena by means of the analysis whether one of them exerts causal influence on another. *TSI* data is actually obtained from Earth Radiation Budget Satellite (*ERBS*)[21]. For this *TSI* we have the data from October 25, (1984) to October 15, (2003) with 14 days interval (with some gaps) whereas *FD* indices (*FDI*) have been generated in *IZMIRAN*, Russia ranging from January 1, (1967) to December 31, (2003) covering almost three full solar cycles simulating the daily mean values from 40-45 neutron monitor stations around the world. The 10*GV* flux of galactic cosmic rays is calculated and then an index on *FD* is introduced, given by I_F[22]. Another index, R_F, is also introduced, which is used for the determination of the *FD* burst related to the response in the near earth space[22]. In the present work we have taken into consideration the index R_F [Source: Belov et al., *IZMIRAN*, Russia and source file: *IF*27*sRF*_list].

Granger causality[23] is an effective instrument to identify the causal influence between two signals. For continuous signals, *e.g.* Electroencephalogram (*EEG*) and local field potential (*LFP*), recent work has shown that Granger causality is suited for this purpose[24-30]. In particular, directional information afforded by Granger causality can play a key role in generating testable hypothesis regarding the finding of source and sink.

However, all the existing approaches assume that the signal observations are obtained at equally spaced time stamps and fail in analyzing irregular signal. Irregularly sampled signals are those with samples missing at blocks of sampling points or collected at non-uniformly spaced time interval. It is a common challenge in practice due to natural constraints or human factors. In summary, there can be two types of irregular signals: gappy signals and non-uniformly sampled signals. Gappy

signal refers to that with regular sampling rate but having many blocks of data missing. For example, in astronomy, a telescope's sight could be blocked by a cloud or celestial obstacles for certain period of time, which makes the recorded samples unavailable during that time[31]. Non-uniformly sampled signal refers to that with observations at non-uniform time points. For example, in health care applications patients usually have difficulties in rigorously recording daily (or weekly) health conditions or pill-taking logs for a long period of time[32]. Here in the present case the problem appears in this connection as the present *TSI* data is gappy in nature. To remove the problem the first task is to reconstruct the *TSI* data in the form of regular-spaced signal. It is also necessary in this regard to reconstruct it with one day interval in order to ensure its comparative study with daily *FDI* data.

We face one more problem in this regard. The stationary characteristics of the *FDI* have been already interpreted[19] whereas in case of TSI the result has been obtained as nonstationary. This creates problem in the process of testing Granger causality between these two signals and to overcome this problem we have to adapt here non-parametric Granger causality test[33,34]. As both the signals may be contaminated with different kind of noise or unwanted information, we have at the first level processed both of them by Savitzky-Golay filter[35] for further analysis. In the present paper, to serve our purpose we have considered the overlapping time period between the present two signals for causality analysis.

2. Theory

(*a*) *Savitzky-Golay nonlinear phase filter:*

Savitzky and Golay[35] proposed a method of data smoothing based on local least-squares polynomial approximation. They showed that fitting a polynomial to a set of input samples and then evaluating the resulting polynomial at a single point within the approximation interval is equivalent to discrete convolution with a fixed impulse response. Considering the group of $(2M+1)$ samples centered at $n = 0$, we obtain the coefficients of a polynomial-

$$p(n) = \sum_{k=0}^{n} a_k n^k \qquad \ldots \quad (1)$$

that minimize the mean-squared approximation error for the group of input samples centered on $n = 0$,

$$y(n) = \sum_{n=-m}^{m} (p(n) - x[n])^2$$

$$= \sum_{n=-m}^{m} (\sum_{k=o}^{n} a_k n^k - x[n])^2 \qquad \ldots \quad (2)$$

The analysis is the same for any other group of $(2M + 1)$ input samples. We shall refer to m as the "half width" of the approximation interval. The smoothed output value is obtained by evaluating $p(n)$ at the central point $n = 0$. That is, $y(0)$, the output at $n = 0$, is

$$y\,[0] = p(0) = a_0 \qquad \ldots \quad (3)$$

so that the output value is just equal to the 0^{th} polynomial coefficient.

This leads to nonlinear phase filters, which can be useful for smoothing at the ends of finite-length input sequences. The output at the next sample is obtained by shifting the analysis interval to the right by one sample, redefining the origin to be the position of the middle sample of the new block of $(2M+1)$ samples, and repeating the polynomial fitting and evaluation at the central location. This can be repeated at each sample of the input, each time producing a new polynomial and a new value of the output sequence $y[n]$. Savitzky and Golay[35] showed that at each position, the smoothed output value obtained by sampling the fitted polynomial is identical to a fixed linear combination of the local set of input samples; *i.e.*, the set of $(2M + 1)$ input samples within the approximation interval are effectively combined by a fixed set of weighting coefficients that can be computed once for a given polynomial order N and approximation interval of length $(2M+1)$. That is, the output samples can be computed by a discrete convolution of the form:

$$y\,[0] = \sum_{n=-m}^{m} h[m]x[n-m]$$
$$= \sum_{m=n-M}^{n+M} h[n-m]x[m] \quad \ldots \quad (4)$$

(b) Non-parametric Granger causality test:

The Granger causality test is used to understand whether a signal influences another signal or in other words whether a signal can be employed to forecast another signal[23]. Primarily, by regression we can have only the measure of correlation between two signals. But that measure is without any orientation *i.e.* if one signal (*A*) is found to be highly correlated with another signal (*B*) using simple cross correlation we cannot determine whether *A* is influencing *B* or the reverse. In case of high magnitude of cross correlation coefficient we can have the following possibilities[23] :

1. *A* may be causing *B*.
2. *B* may be causing *A*.
3. There can be another signal *C* which may be causing both *A* and *B*.
4. There may be a mixed influence of all the above three cases.

So only the information that two signal *A* and *B* are correlated cannot give us any sufficient knowledge about the direction of influence. Granger worked in this particular domain and he proposed a certain test which can successfully divulge this causality. A signal *A* is said to Granger-cause another signal *B* by means of a series of statistical tests if different lagged values of *A* can be used effectively to forecast the future values of *B*[23].

If one of the signals is stationary the test is carried out using the level values of two (or more) variables. If all the variables are non-stationary the test is done using first (or higher) differences as required. In this instant, any particular lagged value of one of the variables can be preserved if the following two incidents are synchronized : (*i*) the present value is statistically significant and (*ii*) the current lagged value together with the

other lagged values adds explicatory power to the model. The null hypothesis of no Granger causality is accepted if and only if no lagged value is kept in the regression. So Granger causality can be expected if at least one lagged value is surely to be retained in the regression.

Though linear Granger causality tests have good potentials in delving into linear causal relation between two variables, their efficiency to extract any form of nonlinearity bin this causal relation may be feeble[36,37]. That's why linear Granger causality tests might fail to notice the nonlinear aspects in the causal relationship between two variables. This indicates that a modified version of linear granger causality analysis is required to understand the nonlinear association between two variables.

Diks and Panchenko[33,34] used a conditional dependence measure by incorporating a local weighting function and their method is summarized below.

In a bivariate system $\{(X_t, Y_t)\}$, X is supposed to Granger cause Y, if the distribution of Y_t for given past observations of X and Y, varies from the distribution of Y_t for given past observations of Y only[23,33,34]. If the information contained in any past observations X_s and Y_s ($s < t$) are considered as $F_{X,t}$ and $F_{Y,t}$ respectively, then we can formulate that $\{X_t\}$ is a nonlinear Granger cause of $\{Y_t\}$ if $Y_t|(F_{X,t}, F_{Y,t}) \sim Y_t|F_{Y,t}$ where "$\sim$" denotes equivalence of distributions [33, 34].

In this process we set up the null hypothesis as [23]

H_0 : $\{X_t\}$ does not Granger cause $\{Y_t\}$.

A uniform marginal density is considered for better performance and in that process a test statistic T_n [33, 34] is employed and this test statistic T_n is given by

$$T_n = \frac{(n-1)}{n(n-2)} \sum_i (C_i^{XYZ} C_i^{Y} - C_i^{XY} C_i^{YZ}) \quad \ldots \quad (5)$$

for a triplet (x,y,z) where n is the size and C stands for local correlation integral. It can be seen that[33,34]

$$\sqrt{n}\frac{[T_n - (2\varepsilon)^m \breve{q}]}{S_n} \xrightarrow{d} N(0,1) \quad \ldots \quad (6)$$

Here S_n is the autocorrelation consistent estimator of variance and ε is the corresponding optimal bandwidth often following a power law as [33, 34]

$$\varepsilon = kn^{-\alpha} \quad \ldots \quad (7)$$

where k is a constant and $\alpha \in \left(\frac{1}{4}, \frac{1}{3}\right)$

and also

$$\breve{q} = (2\varepsilon)^{-d_X - 2d_Y - d_Z} T_n \quad \ldots \quad (8)$$

3. Results

First we have employed Savitzky-Golay filter on both *TSI* and *FDI* data. The original *TSI* and *FDI* data are shown in Fig. 1(*a*) and 2(*a*) respectively. The filtered data for *TSI* and *FDI* after employing Savitzky-Golay filter are demonstrated in Fig. 1(*b*) and 2(*b*) respectively. For the present analysis we have considered the overlapping time period between *TSI* and *FDI*. Here we have identified that the observation period of *TSI* completely falls within the observation period of *FDI*. So we take the overlapping time region accordingly as between October 25, (1984) and October 15, (2003) taking size of each signal as (6818).

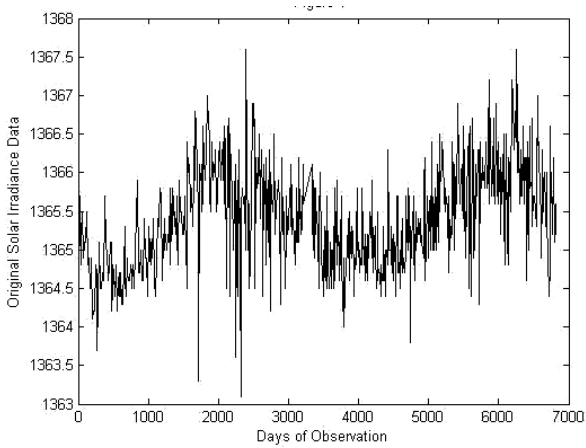

Figure 1(*a*)
Original *TSI* data.

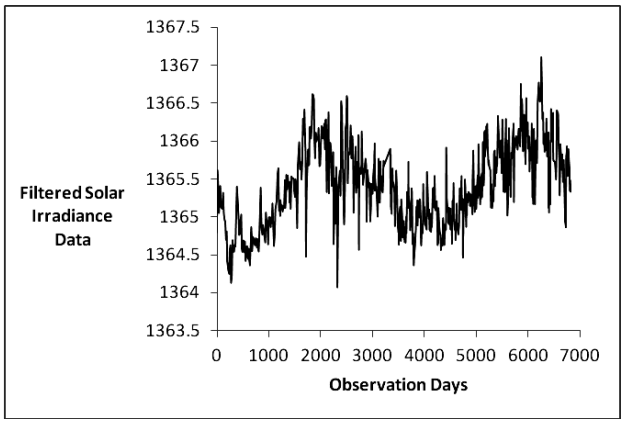

Figure 1(*b*)
Filtered *TSI* Data.

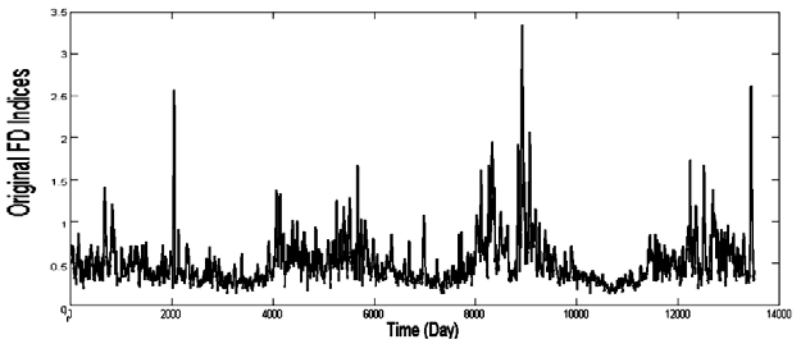

Figure 2(*a*)
Original *FDI* Data.

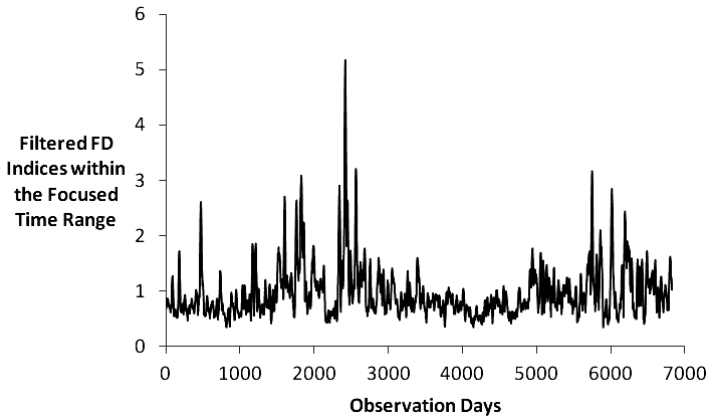

Figure 2(*b*)
Filtered *FDI* Data.

To reconstruct the gappy *TSI* data in the form of a signal with regular one day interval we have first applied Date Compensated Discrete Fourier Transform (*DCDFT*)[38] on it to generate the corresponding power spectrum. Next we have applied Inverse Discrete Fourier Transform (*IDFT*) to generate our desired regular signal[39]. Finally we have gone for the modified Granger causality analysis by means of T_n test statistic[33,34] between the *IDFT* of *TSI* data and *FDI* data and the corresponding result is shown in Table 1. For both the signals we have taken the lag as 1 and therefore the embedding dimension as 2. In the present case for the size n= 6818 as per the prescription in[34] we take the constant k used in (7) as (8). The optimal bandwidth (ε) is taken between 0.50 and 0.65 with regular increment 0.01 suitably adjusting the values of α within the range $(\frac{1}{4}, \frac{1}{3})$.

Firstly we test whether *TSI* Granger causes *FDI* and for that we set up the null hypothesis as $H_0^{(1)}$: '*TSI* does not Granger cause *FDI*' and secondly we check the reverse *i.e.* whether *FDI* Granger causes *TSI* and for that we set the null hypothesis as $H_0^{(2)}$: '*FDI* does not Granger cause *TSI*'. We produce the Table 1 exhibiting the *p*-values for all such cases.

In the statistical hypothesis tests, the *p*-value is the probability for a specified statistical model that, when the null hypothesis is true, the statistical summary as obtained from the considered sample will be the same as or of greater magnitude than the genuine observed results[40]. A small *p*-value (≤ 0.05) designates strong evidence against the null hypothesis and in this situation we reject the null hypothesis. A large *p*-value (> 0.05) furnishes weak evidence against the null hypothesis and hence we fall short to reject the null hypothesis.

Table 1

To test whether *TSI* Granger causes *FDI* or reverse for the embedding dimension 2 and for different optimal bandwidth in the range 0.50-0.65

Optimal bandwidth (ε)	*p*-value for $H_0^{(1)}$: *TSI* does not Granger cause *FDI*	*p*-value for $H_0^{(2)}$: *FDI* does not Granger cause *TSI*
0.50	0.00384	0.05982
0.51	0.00355	0.06029
0.52	0.00334	0.06025
0.53	0.00306	0.05745
0.54	0.00266	0.05412
0.55	0.00259	0.06795
0.56	0.00262	0.07090
0.57	0.00202	0.06561
0.58	0.00217	0.06351
0.59	0.00225	0.05923
0.60	0.00225	0.05484
0.61	0.00214	0.05264
0.62	0.00228	0.05008
0.63	0.00184	0.04582
0.64	0.00182	0.04203
0.65	0.00133	0.04071

From Table 1 it is quite clear that in the first test for all the chosen bandwidths the corresponding *p*-values are very much less than 0.05

whereas for the second test in thirteen out of sixteen cases *p*-values exceed 0.05. This leads us to conclude that the first null hypothesis can be rejected but the second one should be accepted. This in turn points to the possibility that Total Solar Irradiance may Granger cause Forbush decrease but the reverse might not occur.

4. Discussion

In the present work we have undergone Granger causality analysis between *TSI* and *FDI* data in order to investigate if there is any statistical association between them and if yes whether there is any directionality of this association. In other words, the present work is an attempt to identify a relation between the solar-terrestrial climate and cosmic ray intensity.

The observed result shows a prominent statistical association between the present two signals and moreover indicates a possible influence of *TSI* on *FDI*. This in turn fuels the possibility that solar activity may have a significant influence on a drop of cosmic ray intensity. This result supports the experimental evidence produced by Shah et al.[6] that major *FD* can be caused by an extremely high activity of the Sun. In addition to this the present result may also indicate a possibility that Earth's climate influences the *FDI* capture rate. But we do not have any direct evidence in this connection at present. Further investigation is required to venture on this possibility.

At the end we must state one limitation of this work regarding the non-exhibition of the recent profile of the relation between *TSI* and *FDI*. The present work furnishes the relationship based on the data only between October 25, (1984) and October 15, (2003). Though *ERBS* may not be functioning now-a-days but there are certain other sources to have the reading of *TSI* till date. Hence recent data of *TSI* is very much available. But problem lies in the nature of availability of recent *FDI* data. As mentioned earlier, in the present work we have taken into consideration the index R_F for *FDI* which is used for the determination of the *FD* burst related to the response in the near earth space and the same has been simulated by

IZMIRAN capturing the daily mean values from 40-45 neutron monitor stations around the world. Although there are certain communications[41,42,43,44] providing the magnitudes of *FD* at different discrete dates of occurrence covering second half of solar cycle 23 and a large part of solar cycle 24 but the occurrence number is too feeble compared to the actual range of time covered to make any kind of statistical inference. Even in the 'Catalogue of the Forbush-effects and interplanetary disturbances' provided by *IZMIRAN* (Source : http://spaceweather.izmiran.ru/eng/fds2016.html) we can find that there are 1552 events of Forbush effect with very uneven gaps out of possible 5114 days altogether during the time range from January, (2004) to December, (2017). This again gives us the information of only 30% of the entire time period covered. More importantly, these magnitudes do not indicate the index R_F for *FDI* which we have used for our present calculation. On the other hand we have *TSI* data within this range at regular interval. So any statistical approach mingling the regularly available *TSI* data and the sparsely and irregularly arranged data of *FD* effect during this time period should not generate any reliable inference. Further statistical investigation in this direction can be made to have a better insight of this association between *TSI* and *FD* during the second half of solar cycle 23 and a large part of solar cycle 24 only after the availability of recent daily data of *FDI* more or less with no such gap.

Acknowledgements

We express our sincere gratitude to Dr. A.V. Belov, Dr. R. Buetikofer, Dr. E.A. Eroshenko, Dr. R.T. Gushchina, Dr. V.A. Oleneva, Dr. L.M. Baisultanova, Dr. D. Ivanus, Dr. V.N. Obridko, Dr. B.D. Shelting and Dr. V.G. Yanke from the Institute of Terrestrial Magnetism, Ionosphere and Radio Wave Propagation RAS (IZMIRAN), Russia and Dr. P. Raychaudhuri, (Late) Retired Professor, Department of Applied Mathematics, University of Calcutta, Kolkata, India, for kindly providing the necessary data of Forbush decrease indices. We sincerely acknowledge

the support extended by University Grant Commission, Government of India and Jadavpur University, West Bengal, India. This work is a part of UGC-BSR Research Start up Grant [No- 30-103/2015(BSR)] and Jadavpur University Research Grant.

References

1. Forbush, S.E. – Cosmic-ray Variations, 1937–1952, J. Geophys. Res., **64,** 651 (1958).
2. Gold, T. –Energetic particle fluxes in the solar system and near the earth, Astrophys. J. Suppl. Ser., **4**, 406 (1960).
3. Parker, E.N. – Interplanetary Dynamical Processes. Wiley, New York (1963).
4. Barnden, L. R. – The Large-Scale Magnetic Field Configuration Associated With Forbush Decreases, In Proceedings of the 13th International Cosmic Ray Conference, **Vol. 2,** 1277 (1973).
5. Nishida, A. – Numerical modeling of the energy spectrum of the cosmic ray Forbush decrease, J. Geophys. Res., **88,** 785 (1983).
6. Shah, G. N., Mufti, S., Darzi, M. A. and Ishtiaq, P.M. – Major Forbush Decrease recorded by Lead Free-Neutron Monitor, In Proceedings of 29th International Cosmic Ray Conference, Pune, India, **Vol. 1**(SH2.6), 351 (2005).
7. Ifedili, S.O. – Spacecraft measurement of Forbush decreases in the cosmic radiation, Sol. Phys., **168,** 195 (1996).
8. Ifedili, S.O. – Forbush decreases in the cosmic radiation: measurement of the extent of the modulating region, Planet. Space Sci., **45**, 511 (1997).
9. Ifedili, S.O. –The two-step Forbush decrease: An empirical model, J. Geophys. Res., **109** (12), A02117 (2004).
10. Subramanian, P., Antia, H.M., Dugad, S. R., Goswami, U. D. , Gupta, S.K., Hayashi, Y., Ito, N., Kawakami, S., Kojima, H., Mohanty, P.K., Nayak, P.K., Nonaka, T., Oshima, A., Sivaprasad, K., Tanaka, H. and Tonwar, S.C.−Forbush decreases and turbulence levels at coronal mass ejection fronts, A & A **494**, 1107 (2008).
11. Gray, L. J., Haigh, J. D. and Harrison, R.G. – The Influence of Solar Changes on the Earth's Climate, Hadley Centre Technical Note Series 62 (2005).
12. Lean, J. L. – Cycles and trends in solar irradiance and climate, WIREs Climate Change 1 (1), 111 (2010).
13. Laken, B., Kniveton, D. and Wolfendale, A. – Forbush decreases, solar irradiance variations, and anomalous cloud changes, J. Geophys. Res., **116**, D09201 (2011).

14. Dragić, A.L., Veselinović, N., Maletić, D., Joković, D., Banjanac, R., Udovičić, V. and Aničin, I. – Further investigations into the connection between cosmic rays and climate, http://arxiv.org/ftp/arxiv/papers/1304/1304.7879.pdf (2013).

15. Erlykin, A.D. and Wolfendale, A.W. – The Diurnal Temperature Range for Europe: A Search for Cosmic Ray Forbush Decrease Manifestations and the DTR Periodicities, ISRN Atmospheric Sciences 2013, Article ID 982539, 5 pages (2013).

16. Patra, S. N., Bhattacharya, G., Ghosh, K. and Raychauhuri, P. – Search for periodicities of the solar irradiance data from Earth Radiation Budget Satellite (ERBS) using Rayleigh power spectrum analysis, Astrophys. Sp. Sci., **324** (1), 47 (2009).

17. Patra, S. N., Bhattacharya, G. and Ghosh, K. – Search for periodicities of the solar irradiance data from the Earth Radiation Budget Satellite (ERBS) using the periodogram method, Res. Astronomy and Astrophys., **10** (4), 348 (2010).

18. Hossain, K.M., Ghosh, D.N., Ghosh, K. and Bhattacharya, A.K. – Power Spectrum Analysis in Search for Periodicities in Solar Irradiance Time Series Data from ERBS, J. Engg. Sci. Tech. Rev., **4** (1), 96 (2011).

19. Patra, S.N., Ghosh, K. and Panja, S.C. – Time Variation Analysis of the Daily Forbush Decrease Indices, Astrophys. Sp. Sci., **334** (2), 317 (2011).

20. Ghosh, K. and Raychaudhuri, P. – Time Variations of the Forbush Decrease Data, arXiv:astro-ph/0701860 (2006).

21. http://www.ngdc.noaa.gov/stp/solar/irradiance/erbs.html (2009).

22. Belov, A.V., Buetikofer, R., Eroshenko, E.A., Flueckiger, E.O., Gushchina, R.T., Oleneva, V.A. and Yanke, V.G. – Frequency of Forbush effects as an index of solar activity, In Proceedings of 29th International Cosmic Ray Conference, Pune, India, **Vol. 1** (SH 2.6), 375 (2005).

23. Granger, C. W. J. – Investigating Causal Relations by Econometric Models and Cross-spectral Methods, Econometrica, **37** (3), 424 (1969).

24. Baccala, L.A. and Sameshima, K. – Overcoming the limitations of correlation analysis for many simultaneously processed neural structures, Progress in Brain Research, **130**, 33 (2001).

25. Albo, Z., Di Prisco, G.V., Chen, Y., Rangarajan, G., Truccolo, W., Feng, J., Vertes, R.P. and Ding, M. – Is partial coherence a viable technique for identifying generators of neural oscillations? Biol. Cybern., **90**, 318 (2004).

26. Brovelli, A., Ding, M., Ledberg, A., Chen, Y., Nakamura, R. and Bressler, S.L. – Beta oscillations in a large-scale sensorimotor cortical network: directional influences revealed by Granger causality, Proc. Natl. Acad. Sci. U S A, **101** (26), 9849 (2004).
27. Chen, Y., Rangarajan, G., Feng, J. and Ding, M. – Analyzing multiple nonlinear time series with extended Granger causality, Phys. Lett., A **324**, 26 (2004).
28. Seth, A.K – Causal connectivity of evolved neural networks during behavior, Network Comput. Neural Syst., **16**, 35 (2005).
29. Ding, M., Chen, Y. and Bressler, S. – Granger Causality: Basic Theory and Application to Neuroscience, In Schelter, S., Winterhalder, M. and Timmer, J. (eds) Handbook of signal analysis. Wiley, Wienheim, 438 (2006).
30. Wu, J.H., Liu, X.G. and Feng, J. – Detecting M:N causality in simultaneously recorded data, J. Neurosci. Methods, **167**, 367 (2008).
31. Cuevas-Tello, J.C., Tino, P., Raychaudhury, S., Yao, X. and Harva, M. – Uncovering delayed patterns in noisy and irregularly sampled time series: An astronomy application, Pattern Recog., **43**(3), 36 (2009).
32. Kreindler, D.M. and Lumsden, C.J. – The effects of the irregular sample and missing data in time series analysis, Nonlinear Dynamics Psychol. Life Sci., **10**(2), 187 (2006).
33. Diks, C. and Panchenko, V.–A note on the Hiemstra-Jones test for Granger noncausality, Studies in Nonlinear Dynamics & Econometrics, **9**(2), article 4 (2005).
34. Diks, C. and Panchenko, V. – A new statistic and practical guidelines for nonparametric Granger causality testing, Journal of Economic Dynamics and Control, **30**, 1647 (2006).
35. Savitzky, A. and Golay, M.J.E. – Smoothing and Differentiation of Data by Simplified Least Squares Procedures, Analyt. Chem., **36**(8), 1627 (1964).
36. Baek, E. and Brook, W. – A general test for nonlinear Granger causality: Bivariate model, Technical Report, Iowa State University and University of Wisconsin, Masidon (1992).
37. Himestra, C. and Jones, J.D. – Testing for Linear and Nonlinear Granger Causality in the Stock Price-Volume Relation, Journal of Finance, **49**(5), 1639 (1994).
38. Ferraz-Mello, S. – Estimation of periods from unequally spaced observations, Astron. J., **86**, 619 (1981).
39. Babu, P. and Stoica, P. – Spectral Analysis of Nonuniformly Sampled Data - A Review, Digital Signal Processing, **20**(2), 359 (2010).

40. Wasserstein, R. L. and Lazar, N. A. –The ASA's Statement on p-Values: Context, Process, and Purpose, The American Statistician, **70**(2), 129 (2016).
41. Kristj´ansson, J. E., Stjern, C. W., Stordal, F., Fjæraa, A. M., Myhre, G. and J´onasson, K. – Cosmic rays, cloud condensation nuclei and clouds – a reassessment using MODIS data, Atmospheric Chemistry and Physics, **8**, 7373 (2008).
42. Belov, A. V., Abunin, A. A., Abunina, M. A., Eroshenko, E. A., Oleneva, V. A. and Yanke, V. G. – Density Variations of Galactic Cosmic Rays in Magnetic Clouds, Geomagnetism and Aeronomy, **55** (4), 430 (2015).
43. Lingri, D., Mavromichalaki, H., Belov, A. V., Eroshenko, E. A., Yanke, V. G., Abunin, A. A. and Abunina, M. A. – Forbush Decreases during the DeepMin and MiniMax of Solar Cycle 24, XXV European Cosmic Ray Symposium, Turin, September 4-9, (2016), arXiv:1612.08900v1 [astro-ph.HE] (2016).
44. Lingri, D., Mavromichalaki, H., Belov, A. V., Eroshenko, E. A., Yanke, V. G., Abunin, A. A. and Abunina, M. A. – Solar Activity Parameters and Associated Forbush Decreases During the Minimum Between Cycles 23 and 24 and the Ascending Phase of Cycle 24, Solar Phys., **291** (3), 1025 (2016).

INDIAN JOURNAL OF THEORETICAL PHYSICS, VOL. 66, NOS. 1 & 2, 2018

A cable-connected satellites system : stability in elliptical orbit of centre of mass of the

Sangam Kumar* and Santosh Kumar
*Associate Professor, P. G. Department of Physics, L. S. College,
B. R. A. Bihar University, Muzaffarpur- 842001, Bihar, India
Mobile No.: +91-9905222295
E-mail: kumarsangam.phy@gmail.com

[**Abstract:** Stability of equilibrium position of the motion of a system of two cable-connected artificial satellites under the influence of air resistance, solar radiation pressure, earth's shadow and earth's oblateness is studied. Cable, connecting the two satellites, is light, flexible, inextensible and non-conducting in nature. Elliptical orbit of centre of mass of the system is discussed here. In non-linear motion of the system, one equilibrium position exists when all the perturbations mentioned above act on the system simultaneously. Liapunov's theorem is applied to test the stability of the equilibrium position. We conclude that the equilibrium position is unstable in the sense of Liapunov.]

Key-words: Elliptical Orbit, Equilibrium Position, Stability, Liapunov's Theorem.

1. Introduction

Beletsky and Novikova[2] and Beletsky and Novoorebelskii[3] are the pioneer workers in the area of researches in two cable-connected artificial satellites. They studied motion of a system of two cable-connected artificial satellites in the central gravitational field of force relative to its centre of mass. Singh and Demin[10] and Singh[11] could handle the problem in two and three dimensional cases. Effect of magnetic force on the motion of a system of two cable-connected artificial satellites in orbit was studied by Das et.al.[4]. Stability of equilibrium positions of two cable-connected artificial satellites under the influence of solar radiation pressure, earth's oblateness and earth's magnetic field was studied by Kumar and Bhattacharya[5]. Kumar and Srivastava[6] studied about evolutional and non-evolutional motion of a system of two cable-connected artificial satellites under several perturbations. Works of Akbar and Uddin[1] and Kumar[7] are also reviewed in the present research paper.

We study about stability of equilibrium position of the motion of a system of two cable-connected artificial satellites under the influence of air

resistance, solar radiation pressure, shadow of the earth and earth's oblateness in elliptical orbit. We allow the system to pass through the shadow beam. Shadow of the earth is taken to be cylindrical. The nature of cable is light, flexible, inextensible and non-conducting. Central attractive force of the earth will be the main force and all other forces, being small enough are considered here as perturbing forces. In fact, the present work is a physical and mathematical idealization of real space system. We consider the satellites as material particles. Masses of the satellites are small. Distances between the satellites and other celestial bodies are very large. Therefore, gravitational forces of attraction between the satellites and other celestial bodies including the sun are being neglected.

2. Treatment of the problem

We write a set of equations for motion of the system in rotating frame of reference as Kumar and Kumar[8]

$$X''-2Y'-\frac{3X}{\left(1-e^2\right)^{1/2}}=\beta\frac{\left(2+3e^2\right)}{2\left(1-e^2\right)^{7/2}}X+\left(\frac{B_1}{m_1}-\frac{B_2}{m_2}\right).\frac{\cos\alpha\cos\in\sin\theta_2}{\pi}+\frac{12\mu k_2}{R^5}.\frac{1}{\left(1-e^2\right)^{1/2}}X$$

and

$$Y''+2X'=\beta\frac{\left(2+3e^2\right)}{2\left(1-e^2\right)^{7/2}}Y+\left(\frac{B_1}{m_1}-\frac{B_2}{m_2}\right).\frac{\sin\alpha\cos\in\sin\theta_2}{\pi}$$
$$-\frac{3\mu k_2}{R^5}.\frac{1}{\left(1-e^2\right)^{1/2}}Y-\frac{f}{\left(1-e^2\right)^{3/2}} \quad \ldots \quad (1)$$

Condition of constraint is given by

$$X^2+Y^2\le\left(1-e^2\right)^{3/2} \quad \ldots \quad (2)$$

Also,

$$\rho=\frac{1}{\left(1+e\cos\nu\right)},\beta=\frac{p^3}{\mu}\left(\frac{m_1+m_2}{m_1m_2}\right)\lambda,$$

$$A=\left(\frac{m_1}{m_1+m_2}\right)\left(\frac{Q_1}{m_1}-\frac{Q_2}{m_2}\right)\frac{\mu_E}{\sqrt{\mu\rho}}$$

$$f=\frac{a_1p^3}{\sqrt{\mu p}},a_1=\rho_aR'\left(c_2-c_1\right)\left(\frac{m_1}{m_1+m_2}\right) \quad \ldots \quad (3)$$

m_1 and m_2 = masses of the two satellites, B_1 and B_2 = absolute values of the forces due to the direct solar pressure on m_1 and m_2 respectively and are small, p = focal parameter, μ = product of mass of the earth and gravitational constant, λ = undetermined Lagrange's multiplier, R_e = equatorial radius of the earth, g = force of gravity, Ω = angular velocity of the earth's rotation, α_R = earth's oblateness, e = eccentricity of the orbit of the centre of mass v is the true anomaly of the centre of mass of the system, $\in$ = inclination of the oscillatory plane of the masses m_1 and m_2 with the orbital plane of the centre of mass of the system, α = inclination of the ray, γ = shadow function which depends on the illumination of the system of satellites by the sun rays. If γ is equal to zero, then the system is affected by the earth's shadow. If γ is equal to one, then the system is not within the said shadow. R = modulus of position vector of the centre of mass of the system. θ_2 = angle between the axis of the cylindrical shadow beam and the line joining the centre of the earth and the end point of the orbit of the centre of mass within the earth's shadow, considering the positive direction towards the motion of the system, c_1 and c_2 = Ballistic coefficients, ρ_a = average density of the atmosphere. Prime denotes differentiation with respect to v.

Equations (1) do not contain the time explicit, thus Jacobean integral of the problem exists as Kumar[7].

We multiply the first and second equations of (1) by X' and Y' respectively and add them. Then after we integrate the final equation to get Jacobean integral as

$$\cos\in\sin\theta_2\left(X\cos\alpha+Y\sin\alpha\right)+\frac{3\mu k_2}{R^5}.\frac{1}{\left(1-e^2\right)^{1/2}}\left(4X^2-Y^2\right)-\frac{2fY}{\left(1-e^2\right)^{3/2}}+h \qquad (4)$$

θ_2 = constant and h = constant of integration.

3. Equilibrium solution of the problem

Equilibrium positions of the system are given by the constant values of the co-ordinates in rotating frame of reference.

Let $X = X_1$ = constant, $Y = Y_1$ = constant. … (5)

With the help of (5), the set of equations (1) is written as

$$\frac{3X_1}{\left(1-e^2\right)^{1/2}}+\frac{\beta}{2}\frac{\left(2+3e^2\right)}{\left(1-e^2\right)^{7/2}}X_1+\frac{12\mu k_2}{R^5}\cdot\frac{1}{\left(1-e^2\right)^{1/2}}X_1=-\left(\frac{B_1}{m_1}-\frac{B_2}{m_2}\right)\frac{\cos\in\cos\alpha\sin\theta_2}{\pi}$$

and

$$\frac{\beta}{2}\frac{\left(2+3e^2\right)}{\left(1-e^2\right)^{7/2}}Y_1-\frac{3\mu k_2}{R^5}\cdot\frac{1}{\left(1-e^2\right)^{1/2}}Y_1-\frac{f}{\left(1-e^2\right)^{3/2}}=-\left(\frac{B_1}{m_1}-\frac{B_2}{m_2}\right)\frac{\sin\alpha\cos\in\sin\theta_2}{\pi} \quad (6)$$

The presence of perturbation due to solar pressure clearly indicates that none of the co-ordinates of the equilibrium point may be taken to be zero unless $\left(\frac{B_1}{m_1}-\frac{B_2}{m_2}\right)$ or $\theta_2 = 0$. But these parameters cannot be zero. In addition to this, we are interested only to get the maximum effect of the earth's shadow on the motion of the system. Therefore, we put $\in = 0$ and $\alpha = 0$ in equation (6) and get

$$\frac{3X_1}{\left(1-e^2\right)^{1/2}}+\frac{\beta}{2}\frac{\left(2+3e^2\right)}{\left(1-e^2\right)^{7/2}}X_1+\frac{12\mu k_2}{R^5}\cdot\frac{1}{\left(1-e^2\right)^{1/2}}X_1=-\left(\frac{B_1}{m_1}-\frac{B_2}{m_2}\right)\cdot\frac{\sin\theta_2}{\pi}$$

and

$$\frac{\beta}{2}\frac{\left(2+3e^2\right)}{\left(1-e^2\right)^{7/2}}Y_1-\frac{3\mu k_2}{R^5}\cdot\frac{1}{\left(1-e^2\right)^{1/2}}Y_1=\frac{f}{\left(1-e^2\right)^{3/2}} \quad \ldots \quad (7)$$

Equations in (7) are independent of each other, giving the equilibrium position as

$$[X_1,Y_1]=\left[\frac{-\frac{1}{\pi}\left(\frac{B_1}{m_1}-\frac{B_2}{m_2}\right).\sin\theta_2}{\frac{\beta}{2}\frac{\left(2+3e^2\right)}{\left(1-e^2\right)^{7/2}}+\frac{3}{\left(1-e^2\right)^{1/2}}\left(1+\frac{4\mu k_2}{R^5}\right)},\frac{f}{\frac{\beta}{2}\frac{\left(2+3e^2\right)}{\left(1-e^2\right)^{5}}-\frac{3\mu k_2}{R^5}\cdot\frac{1}{\left(1-e^2\right)^{2}}}\right] \quad \ldots \quad (8)$$

4. Stability of the equilibrium position

We apply Liapunov's theorem[9] to test the stability of the equilibrium position given by (8).

Let us assume that there are small variations in the co-ordinates at the given equilibrium position denoted by δ_1 and δ_2, then we have

$$\begin{aligned} X &= X_1 + \delta_1, Y = Y_1 + \delta_2 \\ \therefore X' &= \delta_1', Y' = \delta_2' \\ \therefore X'' &= \delta_1'', Y'' = \delta_2'' \end{aligned} \quad \ldots \quad (9)$$

Using (9) in the equations (1), we obtain a set of variational equations in the form

$$\delta_1'' - 2\delta_2' - \frac{3(X_1+\delta_1)}{(1-e^2)^{1/2}} = \frac{\beta}{2}\frac{(2+3e^2)}{(1-e^2)^{7/2}}\cdot(X_1+\delta_1) + \left(\frac{B_1}{m_1} - \frac{B_2}{m_2}\right)\cdot\frac{\sin\theta_2}{\pi} + \frac{12\mu k_2}{R^5}\frac{1}{(1-e^2)^{1/2}}(X_1+\delta_1)$$

and

$$\delta_2'' + 2\delta_1' = \frac{\beta}{2}\frac{(2+3e^2)}{(1-e^2)^{7/2}}(Y_1+\delta_2) - \frac{3\mu k_2}{R^5}\cdot\frac{(Y_1+\delta_2)}{(1-e^2)^{1/2}} - \frac{f}{(1-e^2)^{3/2}} \quad \ldots \quad (10)$$

where, $\in = 0, \propto = 0$.

Original equations (1) admit Jacobean integral. Therefore variational equations of motion (10) admit Jacobean integral.

We multiply the first and second equations of (10) by $2\delta_1'$ and $2\delta_2'$ respectively, add them and then integrate the final equation to get the Jacobean integral at the equilibrium position as

$$\delta_1'^2 + \delta_2'^2 + \delta_1^2\left[\frac{-3}{(1-e^2)^{1/2}} - \frac{\beta}{2}\cdot\frac{(2+3e^2)}{(1-e^2)^{7/2}} - \frac{12\mu k_2}{R^5}\cdot\frac{1}{(1-e^2)^{1/2}}\right]$$

$$+ \delta_2^2\left[\frac{3\mu k_2}{R^5}\cdot\frac{1}{(1-e^2)^{1/2}} - \frac{\beta}{2}\cdot\frac{(2+3e^2)}{(1-e^2)^{7/2}}\right] + \delta_1\left[-2\left(\frac{B_1}{m_1} - \frac{B_2}{m_2}\right)\cdot\frac{\sin\theta_2}{\pi} - \frac{24\mu k_2}{R^5}\cdot\frac{1}{(1-e^2)^{1/2}}X_1\right.$$

$$\left. - \beta\frac{(2+3e^2)}{(1-e^2)^{7/2}}X_1 - \frac{6}{(1-e^2)^{1/2}}X_1\right] + \delta_2\left[\frac{6\mu k_2}{R^5}\cdot\frac{1}{(1-e^2)^{1/2}}Y_1 - \beta\frac{(2+3e^2)}{(1-e^2)^{7/2}}Y_1 + \frac{2f}{(1-e^2)^{3/2}}\right] = h_1 \quad (11)$$

h_1 = constant of integration at the equilibrium position h.

We consider Jacobean integral as Liapunov's function $L(\delta_1', \delta_2', \delta_1, \delta_2)$ to test the stability in the sense of Liapunov[9]. Next, we write

$$\cdot\delta_1\left[-2\left(\frac{B_1}{m_1}-\frac{B_2}{m_2}\right).\frac{\sin\theta_2}{\pi}-\frac{24\mu k_2}{R^5}.\frac{1}{\left(1-e^2\right)^{1/2}}X_1-\beta.\frac{\left(2+3e^2\right)}{\left(1-e^2\right)^{7/2}}X_1-\frac{6}{\left(1-e^2\right)^{1/2}}X_1\right]$$

$$+\cdot\delta_2^2\left[\frac{3\mu k_2}{R^5}\frac{1}{\left(1-e^2\right)^{1/2}}-\frac{\beta}{2}.\frac{\left(2+3e^2\right)}{\left(1-e^2\right)^{7/2}}\right]$$

$$+\cdot\delta_1\left[-2\left(\frac{B_1}{m_1}-\frac{B_2}{m_2}\right).\frac{\sin\theta_2}{\pi}-\frac{24\mu k_2}{R^5}.\frac{1}{\left(1-e^2\right)^{1/2}}X_1-\beta.\frac{\left(2+3e^2\right)}{\left(1-e^2\right)^{7/2}}X_1-\frac{6}{\left(1-e^2\right)^{1/2}}X_1\right]$$

$$+\cdot\delta_2\left[\frac{6\mu k_2}{R^5}.\frac{1}{\left(1-e^2\right)^{1/2}}Y_1-\beta\frac{\left(2+3e^2\right)}{\left(1-e^2\right)^{7/2}}Y_1+\frac{2f}{\left(1-e^2\right)^{3/2}}\right] \quad \ldots \quad (12)$$

5. Results and discussions

L is the integral of the system of variational equations (10). Its differential taken along the trajectory of the system must vanish identically. Hence, only condition that the equilibrium position be stable in the sense of Liapunov is that *L* must be positive definite. For making the function (12), a positive definite function, it is necessary that the function does not have terms of first order in the variables whereas the terms of the second order 7 must satisfy the Sylvester's conditions for positive definiteness of quadrative forms. Hence, the sufficient conditions for stability of the equilibrium position are as follows :

(*i*) $$\left[-\frac{3}{\left(1-e^2\right)^{1/2}}-\frac{\beta}{2}.\frac{\left(2+3e^2\right)}{\left(1-e^2\right)^{7/2}}-\frac{12\mu k_2}{R^5}.\frac{1}{\left(1-e^2\right)^{1/2}}\right]>0$$

(*ii*) $$\left[-\frac{\beta}{2}.\frac{\left(2+3e^2\right)}{\left(1-e^2\right)^{7/2}}+\frac{3\mu k_2}{R^5}.\frac{1}{\left(1-e^2\right)^{1/2}}\right]>0$$

$$(iii)\left[-2\left(\frac{B_1}{m_1}-\frac{B_2}{m_2}\right).\frac{\sin\theta_2}{\pi}-\frac{24\mu k_2}{R^5}.\frac{1}{\left(1-e^2\right)^{1/2}}X_1-\beta.\frac{\left(2+3e^2\right)}{\left(1-e^2\right)^{7/2}}X_1-\frac{6}{\left(1-e^2\right)^{1/2}}X_1\right]=0$$

$$(iv)\left[\frac{6\mu k_2}{R^5}.\frac{1}{\left(1-e^2\right)^{1/2}}Y_1-\beta\frac{\left(2+3e^2\right)}{\left(1-e^2\right)^{7/2}}Y_1+\frac{2f}{\left(1-e^2\right)^{3/2}}\right]=0 \qquad \ldots \quad (13)$$

All the four conditions should be identically satisfied simultaneously for stability of the equilibrium position.

6. Conclusion

For stability of the equilibrium position in the sense of Liapunov, Jacobean integral at the equilibrium position must be positive definite. This means that Liapunov's function must be positive definite. But in our problem Liapunov's function is not positive definite. It is based on the fact that all the four conditions for positive definiteness given by (13) are not identically satisfied simultaneously. Therefore we conclude that the equilibrium position is unstable.

Acknowledgement

We are thankful to Prof. R. K. Sharma from Thiruvanathapuram for his encouragement.

References

1. Akbar, M. A. and Uddin, M. S. − Jour. Phy. Sci., Midnapore, **12,** pp. 83-96 (2008).
2. Beletsky, V. V. and Novikova, E. T. − Kosmicheskie Issledovania, **7 (6),** pp. 377-384 (1969).
3. Beletsky, V. V. and Novoorebelskii, A. B. − Inst. Appl. Maths., Acad. Sci. U. S. S. R., Soviet Astronomy, **17(2),** pp. 213-220 (1969).
4. Das, S. K., Bhattacharya, P. K. and Singh R. B. − Proc. Nat. Acad. Sci., India, **46,** pp. 287-299 (1976).
5. Kumar, S. and Bhattacharya, P. K. − Proc. Workshop on Spa. Dynamics and Celestial Mech., Muz., Eds. K. B. Bhatnagar and B. Ishwar, pp. 71-74 (1995).

6. Kumar, S. and Srivastava, U. K. − Narosa pub. House, New Delhi, Chennai, Mumbai, Kolkata, pp. 187-192 (2006).

7. Kumar, S. − Jour. Phy. Sci., Midnapore, **23**, pp. 165-170 (2018).

8. Kumar, S. and Kumar, S. − International Jour. Phy. App. Sci., **05 (07)**, pp. 15-21 (2018).

9. Liapunov, A. M. − Sabrania Sachimeiviya, Moscow (Russian), **2N**, pp. 327 - 335 (1959).

10. Singh, R. B. and Demin, V. G. − Celestial Mech., **06**, pp. 268-277 (1972).

11. Singh, R. B. − Astronautica Acta, **18,** pp. 301-308 (1973).

INDIAN JOURNAL OF THEORETICAL PHYSICS, VOL. 66, NOS. 1 & 2, 2018

Effects of induced magnetic field and thermal radiation on visco-elastic fluid flow past an infinite vertical porous plate with constant heat flux

Paban Dhar
Department of Mathematics, Karimganj College, Assam, India
E-mail: pabankumardhar@yahoo.com

and

Rita Choudhury
Department of Mathematics, Gauhati University, Assam, India
E-mail: rchoudhury66@yahoo.in

[Abstract : The effects of induced magnetic field on steady mixed convective flow over a vertical porous plate with constant heat flux in presence of thermal radiation has been investigated. The fluid is assumed to be visco-elastic, electrically conducting and incompressible. The visco-elastic fluid flow is characterized by Walters liquid (Model B'). Using Boussinesq and boundary layer approximation, the nonlinear governing equations of motion are formulated. Analytical solutions of these equations are obtained with the help of regular perturbation technique. Also, the graphical illustrations of the solutions have been presented with different values of physical parameters involved in the problem].

Keywords: Walters liquid (Model B'), *MHD*, Perturbation Technique, Hartmann number, Prandtl number, Thermal radiation.

1. Introduction

The study of mixed convective flow of an electrically conducting fluid with simultaneous heat and mass transfer past a vertical porous surface has many engineering and geophysical applications such as thermal insulation, drying of porous solids, glass fiber production, wire drawing and many others. In recent years, various aspects of these types of problems have been investigated by many authors (Sakiadis[1], Bejan and Khair[2], Pop and Soundalgekar[3], Elashbeshy[4] etc.).

Another important aspect that is magneto-hydrodynamics plays an important role in the context of engineering and aerodynamics. Furthermore, *MHD* convection flow problem with heat and mass transfer are very significant in the fields of astrophysics and geophysics to study the stellar and solar structures, instellar matters etc. Keeping in mind the above applications, numerous attempts have been made to study the effect of transverse magnetic field on flow characteristics (Cowling[5], Sparrow and Cess[6], Riley[7], Crammer and Pai[8], Glauert[9] etc.). Raptis and Soundalgekar[10] in his work have presented a systematic analysis on magnetohydrodynamic free convection flow past a moving porous plate with constant heat flux. Workers like Raptis and Kafousias[11], Kafousias and Georgantopoulos[12], Raptis and Soundalgekar[13], Acharya et al.[14], Singh et al.[15] and Makinde[16] have investigated the effects of magnetic field on convection flow with mass transfer past a vertical surface in presence of constant heat flux and suction. Abdelkhalek[17] has discussed the effect of magnetic field on heat and mass transfer free convection problem and analyzed some interesting theoretical aspects of the solution using perturbation technique. However, all these works have been neglected induced magnetic field which is also one of the important parameter to change the velocity and temperature fields in a fluid flow. Singh and Singh[18] have studied *MHD* effects on heat and mass transfer in a viscous fluid taking into account the induced magnetic field. Ahmed[19] has presented an analytical study of induced magnetic field with radiating fluid over a porous vertical plate. Also, Ahmed et al.[20] have studied the effects of *MHD* mixed convection and mass transfer past a vertical porous plate with chemical reaction by considering induced magnetic field and heat source.

Non-Newtonian fluid flows arise in numerous processes in chemical engineering systems such as drawing of plastic films, liquid films in condensation process, filament extrusion from a dye etc. Since most of the industrially important fluids such as molten plastics, polymers, pulps etc. associated in these applications are more visco-elastic in nature than viscous. Due to growing use of these types of fluids in various manufacturing and processing industries, the studies related to visco-elastic

fluids have gained momentum towards understanding their flow behavior. Many authors have developed several mathematical models to study the diverse hydrodynamic behaviors of visco-elastic fluids. Many of the visco-elastic fluids encountered in chemical engineering processes are known to follow the so called Walters liquid (Model B') developed by Walters[21]. This is one kind of visco-elastic fluid which resists shear flow and strains linearly with time under the application of an applied stress but when the stress is removed it quickly returns to its original position.

In certain practical problems, the motion of visco-elastic fluid with heat and mass transfer over a vertical surface in presence of magnetic field have been investigated by several authors like Choudhury and Deb[22], Siddappa and Abel[23], Subhas et al.[24]. Sonth et al.[25] have studied the heat and mass transfer in a visco-elastic fluid flow over an accelerating surface with heat source/sink and viscous dissipation. Visco-elastic fluid flow with the presence of magnetic field past a porous circular cylinder has been studied by Widodo et al.[26]. Choudhury and Das[27] have discussed flow and heat transfer in *MHD* visco-elastic fluid with ohmic heating. Also, Visco-elastic *MHD* flows and heat transfer over a stretching sheet with viscous and ohmic dissipations has been investigated by Abel et al.[28]. The effects of hall current and radiation on visco-elastic fluid flow with heat and mass transfer past a vertical porous plate have been studied by Choudhury et al.[29]. Choudhury and Das[30] have investigated the influence of visco-elasticity on *MHD* heat and mass transfer flow through a porous medium bounded by an inclined surface with chemical reaction.

The aim of the present investigation is to study the effect of induced magnetic field and radiation on two dimensional steady visco-elastic flows past an infinite vertical porous plate with constant heat flux in presence of viscous dissipation. The governing nonlinear momentum and energy equations are solved analytically using regular perturbation technique. The inclusion of visco-elastic fluid characteristics to the previous studies done by Ahmed[19] and Ahmed et al.[20] leads to some interesting effects on both the velocity and temperature fields.

The constitutive equation for Walters liquid (Model B') is

$$\sigma_{ik} = -pg_{ik} + \sigma'_{ik},$$
$$\sigma'^{ik} = 2\eta_0 e^{ik} - 2k_0 e'^{ik} \quad \ldots \quad (1)$$

where σ^{ik} is the stress tensor, p is isotropic pressure, g_{ik} is the metric tensor of a fixed co-ordinate system x^i, v_i is the velocity vector, the contravarient form of e'^{ik} is given by

$$e'^{ik} = \frac{\partial e^{ik}}{\partial t} + v^m e^{ik}_{,m} - v^k_{,m} e^{im} - v^i_{,m} e^{mk}, \quad \ldots \quad (2)$$

It is the convected derivative of the deformation rate tensor e^{ik} defined by

$$2e^{ik} = v_{i,k} + v_{k,i} \quad \ldots \quad (3)$$

Here η_0 is the limiting viscosity at the small rate of shear which is given by

$$\eta_0 = \int_0^\infty N(\tau)d\tau \text{ and } k_0 = \int_0^\infty \tau N(\tau)d\tau \quad \ldots \quad (4)$$

$N(\tau)$ being the relaxation spectrum. This idealized model is a valid approximation of Walters liquid (Model B') taking very short memories into account so that terms involving

$$\int_0^\infty t^n N(\tau)d\tau, \ n \geq 2 \quad \ldots \quad (5)$$

have been neglected.

2. Mathematical formulation

We consider a steady mixed convective *MHD* flow of a laminar, incompressible, electrically conducting visco-elastic fluid past an infinite vertical porous plate with constant heat flux by considering induced magnetic field as well as radiation effect. The effect of energy dissipation due to viscosity has been considered in this problem. The flow is two-dimensional where x' axis is taken along the plate, being the vertically upward direction of the motion and y' is taken normal to the plate directed into the fluid. A uniform magnetic field of strength B_0 is applied normal to the plate. Since the plate is considered infinite in the x' direction, hence all the fluid properties are independent of x' axis. Let u' and v' be the fluid

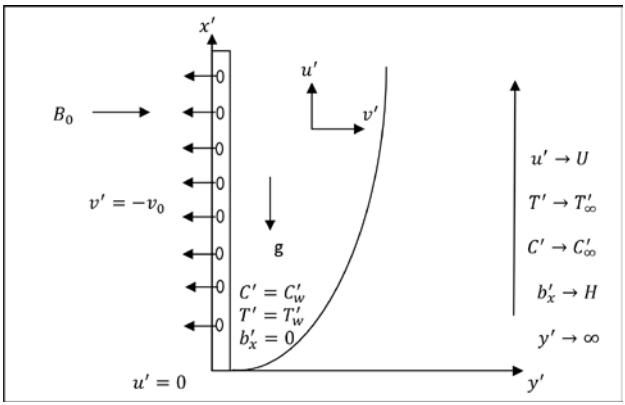

Figure 1

Physical configuration and coordinate system.

velocities along x' and y' axis respectively. Then under Boussinesq's and boundary layer approximation the equations of motion governing such type of flow are:

Equation of Continuity :

$$\frac{\partial v'}{\partial y'} = 0 \text{ which is satisfied with } v' = -v_0, \text{ a constant} \quad \ldots \quad (6)$$

Momentum equation :

$$v'\frac{\partial u'}{\partial y'} = \nu\frac{\partial^2 u'}{\partial y'^2} + g\beta\left(T' - T'_\infty\right) + g\beta'\left(C' - C'_\infty\right) - \frac{k_0}{\rho}v'\frac{\partial^3 u'}{\partial y'^3} + \frac{\eta\sigma B_0}{\rho}\frac{\partial b_x'}{\partial y'} \quad \ldots \quad (7)$$

Energy equation :

$$v'\frac{\partial T'}{\partial y'} = \frac{K_T}{\rho C_p}\frac{\partial^2 T'}{\partial y'^2} + \frac{\eta_0}{\rho C_p}\left(\frac{\partial u}{\partial y'}\right)^2 - \frac{k_0}{\rho C_p}\left(v'\frac{\partial u'}{\partial y'}\frac{\partial^2 u'}{\partial y'^2}\right) - \frac{1}{\rho C_p}\frac{\partial q_r'}{\partial y'} + \frac{\sigma\eta^2}{\rho C_p}\left(\frac{\partial b_x'}{\partial y'}\right)^2 \ldots \quad (8)$$

Magnetic induction equation :

$$\eta\frac{\partial^2 b_x'}{\partial y'^2} + B_0\frac{\partial u'}{\partial y'} - v'\frac{\partial b_x'}{\partial y'} = 0 \quad \ldots \quad (9)$$

Species continuity equation :

$$v'\frac{\partial C'}{\partial y'} = D\frac{\partial^2 C'}{\partial y'^2} \quad \ldots (10)$$

The relevant boundary conditions are :

$$y' = 0 : u' = 0,\ v' = -v_0 = \text{constant},\ \frac{\partial T'}{\partial y'} = -\frac{q}{K_T}, C' = C_w', b_x' = 0$$

$$y' \to \infty : u' \to U', \quad T' \to T'_\infty, \quad C' \to C'_\infty, b_x' \to H' \quad \ldots (11)$$

We introduce the following non-dimensional quantities :

$$y = \frac{y'v_0}{\nu}, u = \frac{u'}{v_0}, U = \frac{U'}{v_0}, b_x = \frac{b_x'}{B_0}, H = \frac{H'}{B_0}, \theta = \frac{K_T v_0 (T' - T_\infty')}{q\nu}, \phi = \frac{(C' - C_\infty')}{(C_w' - C_\infty')}$$

$$Gr = \frac{g\beta\nu^2 q}{K_T v_0^4}, Gm = \frac{g\beta'\nu\,(C_w' - C_\infty')}{v_0^3}, M = \frac{\sigma B_0^2 \nu}{\rho v_0^2}, Pr = \frac{\eta_0 C_p}{K_T}, Pm = \frac{\nu}{\eta},$$

$$Sc = \frac{\nu}{D}, k = \frac{k_0 v_0^2}{\rho\nu^2}, R = \frac{64a\nu\bar{\sigma}T_\infty'^4}{\rho v_0^2 C_p}, \qquad Ec = \frac{U^2 K_T v_0}{q\nu C_p}$$

where *Gr* is the thermal Grash of number, *Gm* is the solutal Grashof number, *M* is the magnetic parameter, *Pr* is the Prandtl number, *Pm* is the magnetic Prandtl number, *Sc* is the Schmidt number, *k* is the visco-elastic parameter and *R* is the radiation parameter.

In case of an optically thin gray gas, the local radiant absorption is expressed as

$$\frac{\partial q_r'}{\partial y'} = -4a\bar{\sigma}\left(T_\infty'^4 - T'^4\right) \qquad \ldots \quad (12)$$

where $'a', \bar{\sigma}$ are the absorption coefficient and Stefan-Boltzmann constant respectively. It is assumed that the temperature differences within the flow are sufficiently small such that T'^4 may be expressed as linear function of the temperature T'. This is accomplished by expanding T'^4 in Taylor series about T_∞' and neglecting higher order terms, thus

$$T'^4 \cong 4T_\infty'^3 T' - 3T_\infty'^4 \qquad \ldots \quad (13)$$

Using the non-dimensional quantities and with the help of (12) and (13), the dimensionless governing equations of motion are

$$-\frac{du}{dy} = \frac{d^2u}{dy^2} + Gr\theta + Gm\phi + \frac{M}{Pm}\frac{db_x}{dy} + k\frac{d^3u}{dy^3} \qquad \ldots \quad (14)$$

$$-\frac{d\theta}{dy} = \frac{1}{Pr}\frac{d^2\theta}{dy^2} + Ec\left(\frac{du}{dy}\right)^2 + kEc\frac{du}{dy}\frac{d^2u}{dy^2} + \frac{MEc}{Pm^2}\left(\frac{db_x}{dy}\right)^2 + \frac{R\theta}{4} \qquad \ldots \quad (15)$$

$$\frac{d^2b_x}{dy^2} + Pm\frac{du}{dy} + Pm\frac{db_x}{dy} = 0 \qquad \ldots \quad (16)$$

$$\frac{d^2\phi}{dy^2} + Sc\frac{d\phi}{dy} = 0 \qquad \ldots \quad (17)$$

Subject to the boundary conditions

$$y = 0:\ u = 0\,,\qquad \frac{\partial\theta}{\partial y} = -1\,,\ \phi = 1\,,\ b_x = 0$$

$$y \to \infty:\ u \to U,\ \theta \to 0, \phi \to 0,\ \ b_x = H \qquad \ldots \quad (18)$$

3. Method of solution

The solution of the equation (17) subject to the boundary conditions (18) is

$$\phi = e^{-Scy}$$

Now, in order to solve the equations (14) - (16) under the relevant boundary conditions given by (18), it is assumed that the solutions of the equations to be of the form :

$$u = u_0 + Ecu_1 + Ec^2u_2 + \cdots$$

$$\theta = \theta_0 + Ec\theta_1 + Ec^2\theta_2 + \cdots$$

$$b_x = b_{x_0} + Ecb_{x_1} + Ec^2b_{x_2} + \cdots \qquad \ldots \quad (19)$$

where *Ec* is the Eckert number (*Ec* << 1, for incompressible fluids). Substituting (19) in the equations (14) - (16) and equating the coefficient of the same degree terms and neglecting terms of $O(Ec^2)$,we get the following differential equations:

$$ku_0''' + u_0'' + u_0' = -Gr\theta_0 - Gm\phi - \frac{M}{Pm}b_{x_0}' \qquad \ldots \quad (20)$$

$$ku_1''' + u_1'' + u_1' = -Gr\theta_1 - \frac{M}{Pm}b_{x_1}' \qquad \ldots \quad (21)$$

$$\theta_0'' + Pr\theta_0' + \frac{PrR}{4}\theta_0 = 0 \qquad \ldots \quad (22)$$

$$\theta_1'' + Pr\theta_1' + Pru_0'^2 + kPru_0'u_0'' + \frac{PrM}{Pm^2}b_{x_0}'^2 + \frac{PrR}{4}\theta_1 = 0 \qquad \ldots \quad (23)$$

$$b_{x_0}'' + Pmb_{x_0}' + Pmu_0' = 0 \qquad \ldots \quad (24)$$

$$b_{x_1}'' + Pmb_{x_1}' + Pmu_1' = 0 \qquad \ldots \quad (25)$$

The transformed boundary conditions is given by

$$y = 0:\ u_0 = 0\,, u_1 = 0, \frac{\partial\theta_0}{\partial y} = -1\,, \frac{\partial\theta_1}{\partial y} = 0,\ b_{x_0} = 0\,,\ b_{x_1} = 0$$

$$y \to \infty:\ u_0 = U, u_1 = 0,\ \theta_0 = 0\,, \theta_1 = 0,\ b_{x_0} = H\,,\ b_{x_1} = 0 \qquad \ldots \quad (26)$$

The solutions of the equations (22) subject to the boundary conditions (26) are given by

$$\theta_0 = A_4 e^{-B_2 y}$$

Again, to solve the equations (20), (21), (23), (24) and (25), we use multi parameter perturbation technique in terms of visco-elastic parameter k (as $k<<1$ for small shear rate). Thus we write

$$u_0 = u_{00} + k u_{01} + O(k^2) \ldots.$$
$$\theta_1 = \theta_{10} + k\theta_{11} + O(k^2) \ldots$$
$$b_{x_0} = b_{x_{00}} + k b_{x_{01}} + O(k^2) \ldots \quad \ldots \quad (27)$$

Using (27) in equations (20), (21), (23), (24) and (25), and equating the coefficient of k^0, k^1 we get the following sets of equations:

$$u_{00}'' + u_{00}' = -Gr\theta_0 - Gm\phi - \frac{M}{Pm} b_{x_{00}}' \quad \ldots \quad (28)$$

$$u_{00}'''' + u_{01}'' + u_{01}' = -\frac{M}{Pm} b_{x_{01}}' \quad \ldots \quad (29)$$

$$u_{10}'' + u_{10}' = -Gr\theta_1 - \frac{M}{Pm} b_{x_{10}}' \quad \ldots \quad (30)$$

$$u_{11}'' + u_{11}' = -\frac{M}{Pm} b_{x_{11}}' - u_{10}'''' \quad \ldots \quad (31)$$

$$\theta_{10}'' + Pr\theta_{10}' + Pru_{00}'^2 + \frac{PrM}{Pm^2} b_{x_{00}}'^2 + \frac{PrR}{4}\theta_{10} = 0 \quad \ldots \quad (32)$$

$$\theta_{11}'' + Pr\theta_{11}' + 2Pru_{00}' u_{01}' + Pru_{00}' u_{00}'' + \frac{2PrM}{Pm^2} b_{x_{00}}' b_{x_{01}}' + \frac{PrR}{4}\theta_{11} = 0$$

$$\ldots \quad (33)$$

$$b_{x_{00}}'' + Pmb_{x_{00}}' + Pmu_{00}' = 0 \quad \ldots \quad (34)$$

$$b_{x_{01}}'' + Pmb_{x_{01}}' + Pmu_{01}' = 0 \quad \ldots \quad (35)$$

$$b_{x_{10}}'' + Pmb_{x_{10}}' + Pmu_{10}' = 0 \quad \ldots \quad (36)$$

$$b_{x_{11}}'' + Pmb_{x_{11}}' + Pmu_{11}' = 0 \quad \ldots \quad (37)$$

The modified boundary conditions are as follows :

$$y = 0:\ u_{00} = u_{01} = u_{10} = u_{11} = 0\,,$$
$$\frac{\partial \theta_{10}}{\partial y} = 0\,, \frac{\partial \theta_{11}}{\partial y} = 0,\ b_{x_{00}} = b_{x_{01}} = b_{x_{10}} = b_{x_{11}} = 0$$
$$y \to \infty:\ u_{00} = U, u_{01} = u_{10} = u_{11} = 0,$$
$$\theta_{10} = \theta_{11} = 0,\ b_{x_{00}} = H\,,\ b_{x_{01}} = 0,\ b_{x_{10}} = b_{x_{11}} = 0 \quad \ldots (38)$$

Solutions of the equations (28) to (37) subject to the boundary conditions (38) are obtained but not presented here for the sake of brevity.

Shearing stress, Rate of heat transfer and Rate of mass transfer :

The non-dimensional shearing stress τ at the plate y=0 is given by

$$\tau = \left(\frac{\partial u}{\partial y} + k\frac{\partial^2 u}{\partial y^2}\right)_{y=0} \quad \ldots \quad (39)$$

The non-dimensional heat flux at the plate y = 0 in terms of Nusselt number Nu is given by

$$Nu = \left[\frac{\partial \theta}{\partial y}\right]_{y=0} = \left\{\frac{\partial \theta_0}{\partial y} + Ec\frac{\partial \theta_1}{\partial y}\right\}_{y=0}$$
$$= -B_2A_4 + Ec[B_1A_{34} - B_2A_{35} + 2B_4A_{64} + (B_2 + B_4)A_{65} + (B_4 + Sc)A_{66} + 2B_2A_{67} + 2ScA_{68} + (B_2 + Sc)A_{69} + (B_4 + 1)A_{79} + (B_2 + 1)A_{80} + (Sc + 1)A_{81} - A_{70} - A_{72} - A_{74} - A_{76} + 2A_{78}] \quad \ldots \quad (40)$$

The non-dimensional mass flux at the plate y = 0 in terms of Sherwood number Sh is given

$$Sh = \left(\frac{d\phi}{dy}\right)_{y=0} = -Sc \quad \ldots \quad (41)$$

4. Results and discussion

The problem of steady state mixed convective hydromagnetic visco-elastic flow of incompressible and electrically conducting visco-elastic fluid

past an infinite vertical porous plate with constant heat flux in presence of thermal radiation and induced magnetic field has been formulated, analyzed and solved by using multi-parameter perturbation technique. Approximate solutions have been derived for velocity, temperature, concentration, shearing stress and induced magnetic field. To assess the effects of visco-elasticity along with the other dimensionless thermo physical parameters on a fluid flow field in the boundary layer region, the numerical values of fluid velocity, temperature, shearing stress and induced magnetic field computed from the analytical solution are discussed graphically in figures 2 -16.

In this section, the non-dimensional parameter k=0 characterizes the Newtonian fluid phenomenon and non zero values of k exhibit the visco-elastic fluid. Figures 2-6 show variations of velocity (u) as function of y for several values of Magnetic number (M), Prandtl number (Pr), Radiation parameter (R), thermal Grashof number (Gr), solutal Grashof number (Gm), Schmidt number (Sc) and visco-elastic parameter (k). It can be observed from these figures that the fluid velocity rises in the neighborhood of the plate but significantly slows down far away from the plate in both Newtonian and non-Newtonian cases. Again, during the modification of visco-elastic parameter, the fluid velocity rises considerably in comparison to Newtonian fluid flow phenomenon.

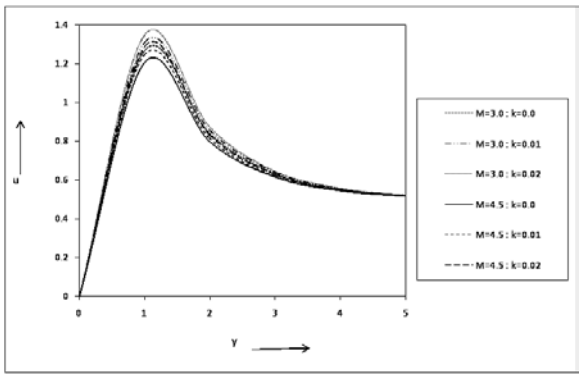

Figure 2
Fluid velocity u against y for Pr=2, Pm=2, Gr=5, Gm=5, Sc=1.5, R=1.5, H=0.5, U=1.

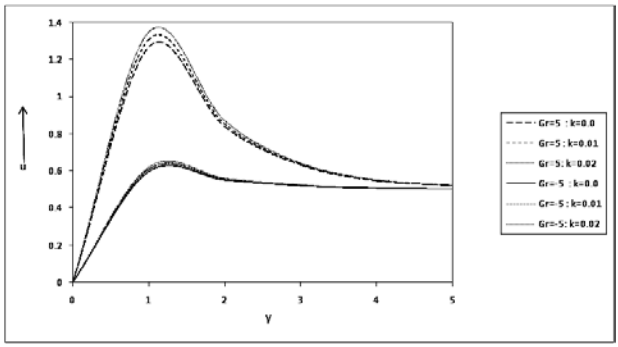

Figure 3
Fluid velocity u against y for M=3, Pr=2, Pm=2, Gm=5
Sc=1.5, R=1.5, H=0.5, U=1.

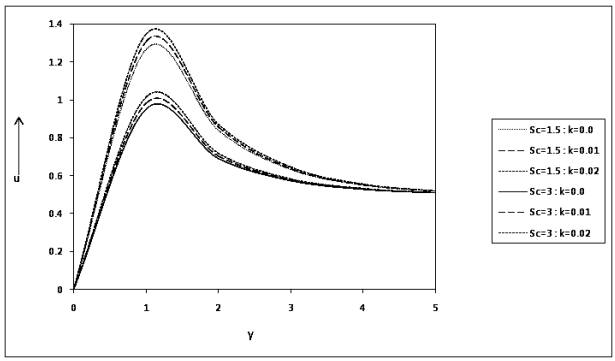

Figure 4
Fluid velocity u against y for M=3, Pr=2, Pm=2,
Gr=5, Gm=5, R=1.5, H=0.5, U=1.

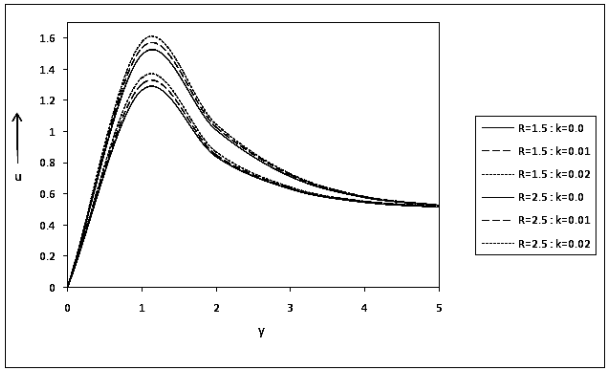

Figure 5
Fluid velocity u against y for M=3, Pr=2, Pm=2,
Gr=5, Gm=5, Sc=1.5, H=0.5, U=1.

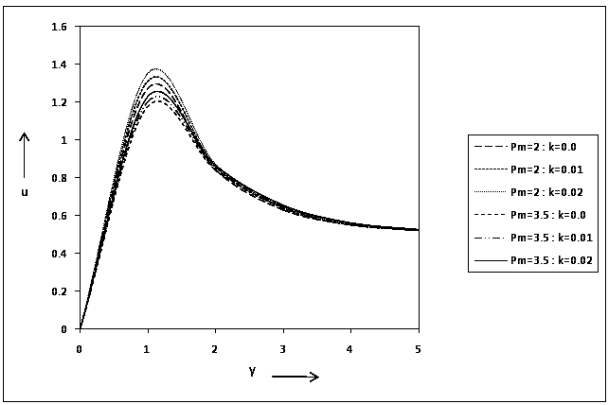

Figure 6
Fluid velocity u against y for M=3, Pr=2, Gr=5, Gm=5, Sc=1.5, R=1.5, H=0.5, U=1.

The effects of the magnetic parameter on the fluid velocity are illustrated in figure 2. The effect of magnetic parameter (M) is seen to decrease the fluid velocity throughout the boundary layer but significantly near the plate. This is because of Lorentz force which is produced due to the application of transverse magnetic field and acts against the motion of the fluid. Physically Gr<0 signifies externally heated plate and Gr>0 signifies externally cooled plate. Figure 3 illustrates that the speed of the fluid flow is enhanced on the cooled plate in comparison with flow past a heated plate. The effects of Schmidt number and radiation parameter on velocity field have been shown in figures 4 and 5 respectively. It can be noticed that the flow is decelerated with an increase in Schmidt number and radiation parameter. This may be concluded to the fact that the presence of Schmidt number and radiation parameter implies less interaction of diffusion species and radiation respectively with the momentum boundary layer. Figure 6 shows the influence of magnetic Prandtl number on velocity field in presence of strong magneto-hydrodynamic flow. The figure reveals that a rise in magnetic Prandtl number causes a noticeable decreasing in the flow velocity, in particular at short distance from the surface of the wall. This is due to the fact that an ascending value of Magnetic Prandtl number raises the friction of the fluid particles which in turn retards the speed of the fluid flow.

Figures 7-10 show the variations of the shearing stress with the changes of visco-elastic parameter against different values of Magnetic parameter (*M*), radiation parameter *R*, Prandtl number *Pr* and Schmidt number *Sc*. Analysis of these graphs reveal that the growth of visco-elastic parameter enhance the magnitude of shearing stress experienced by visco-elastic fluid in comparison with Newtonian fluid. The effect of magnetic parameter on shearing stress is shown in figure 7. It is seen that the increasing values of *M* is to increase shearing stress throughout the boundary layer more significantly. Figure 8 represents the behavior of shearing stress against radiation parameter with other physical parameters. It is noticed that the shearing stress experienced by both fluid systems is accelerated largely with the increase of radiation parameter. Also, it is depicted that initially the magnitude differences between visco-elastic fluid and Newtonian fluid is more prominent in nature but gradually it becomes less prominent with higher values of radiation parameter. The influence of Prandtl number on shearing stress is noticed in figure 9. The figure depicts that the magnitude of shearing stress is increasing with an increase of Prandtl number and achieve its maximum value at *Pr* = 3 and then decreases gradually with higher values of Prandtl number. Figure 10 reveals that shearing stress experienced by both Newtonian and visco-elastic fluid decreases considerably up to the value *Sc* = 2, while the magnitude increases to some extent up to *Sc* = 2.5 and then finally decreases with the enhancement of Schmidt number (*Sc*).

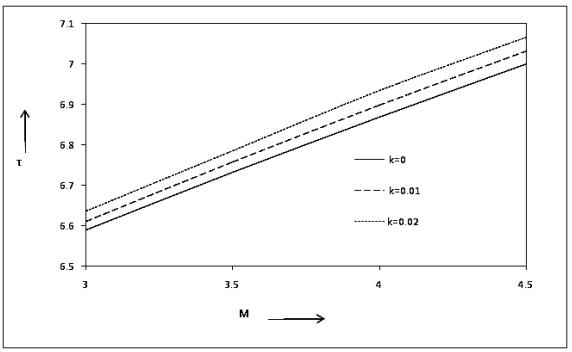

Figure 7
Shearing stress against *M* for *Pm*=2, *Pr*=2, *Gr*=5, *Gm*=5, *Sc*=1.5, *R*=1.5, *H*=0.5, *U*=1.

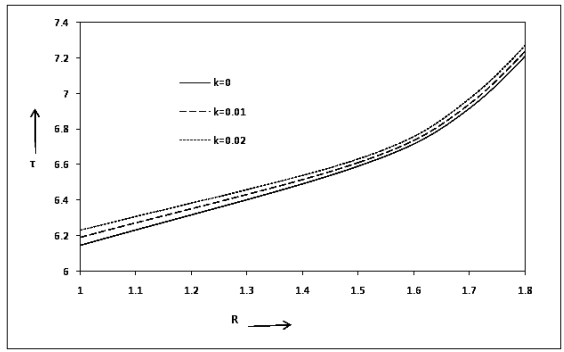

Figure 8
Shearing stress against R for M=3, Pm=2, Pr=2, Gr=5, Gm=5, Sc=1.5, H=0.5, U=1.

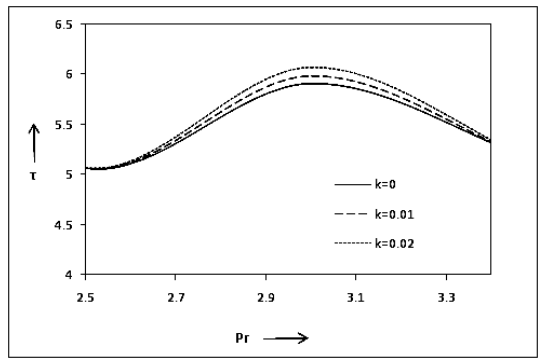

Figure 9
Shearing stress against Pr for M=3, Pm=2, Gr=5, Gm=5, Sc=1.5, R=1.5, H=0.5, U=1.

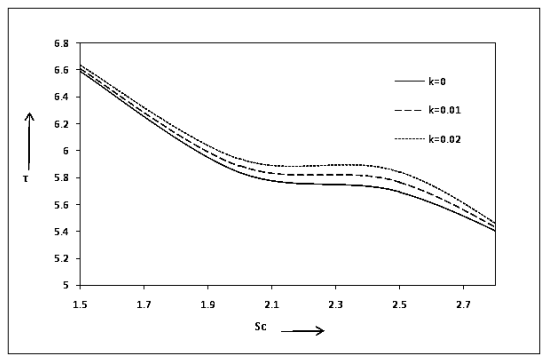

Figure 10
Shearing stress against Sc for M=3, Pm=2, Pr=2, Gr=5, Gm=5, R=1.5, H=0.5, U=1.

Temperature distribution for various values of visco-elastic parameter, radiation parameter and Prandtl number are plotted against y in the figures 11-14. The effects of Prandtl number on temperature fields for visco-elastic fluid are illustrated in figure 11. It is likely to found that temperature profile decreases with y for the variation of Pr, which means that the thermal boundary layer is thinner for large Prandtl number. The similar pattern has been observed in case of Newtonian fluid also (figure 12). Figures 13-14 represent graphs of temperature fields θ for various values of radiation parameter. An increase in the radiation parameter inside the boundary layer leads to higher temperature profile. This is due to the fact that temperature accelerates as radiation parameter grows, which satisfy the physical fact that the thermal boundary layer thickness rises with an increase of radiation parameter (R). Also, it can be concluded that a rise of R from 1.5 to 1.9, raise the temperature near the plate and this increment of temperature would be more in case of visco-elastic fluid as compared to Newtonian fluids.

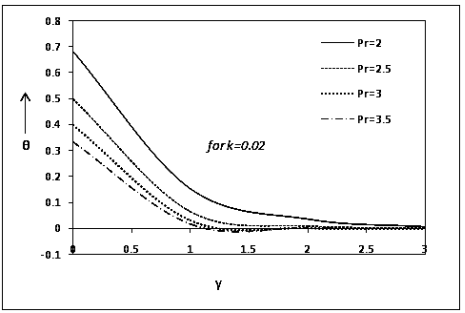

Figure 11
Temperature θ against y for Pm=2, M=3, Gr=5
Gm=5, Sc=1.5, R=1.5, H=0.5, U=1.

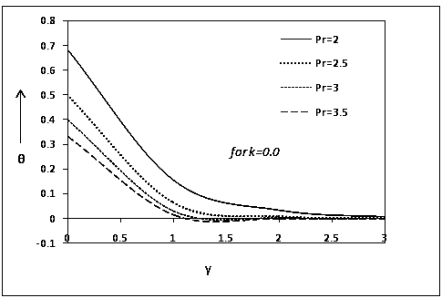

Figure 12
Temperature θ against y for M=3, Pm=2, Gr=5,
Gm=5, Sc=1.5, R=1.5, H=0.5, U=1.

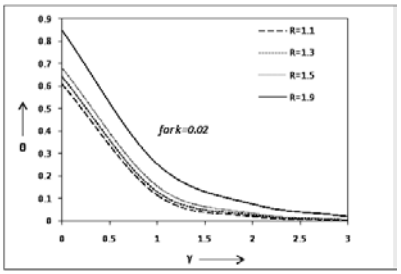

Figure 13
Temperature θ against y for M=3, Pm=2, Pr=2, Gr=5, Gm=5, Sc=1.5, H=0.5, U=1.

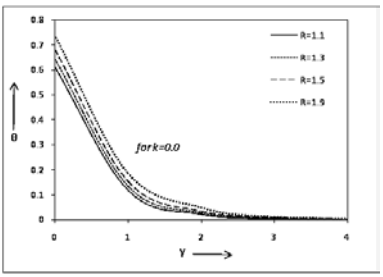

Figure 14
Temperature θ against y for M=3, Pm=2, Pr=2, Gr=5, Gm=5, Sc=1.5, H=0.5, U=1.

Figures 15-16 have been plotted against y to depict the variations of induced magnetic field with the variations of Magnetic parameter and Magnetic Prandtl number for visco-elastic fluids. It has been analyzed from these figures that the magnitude of induced magnetic field increases sharply up to 0.6 due to rising values of M and Pm and then diminishes considerably.

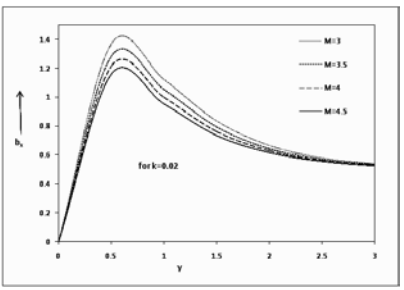

Figure 15
Induced Magnetic field b_x against y for Pm=2, Pr=2, Gr=5, Gm=5, Sc=1.5, R=1.5, H=0.5, U=1.

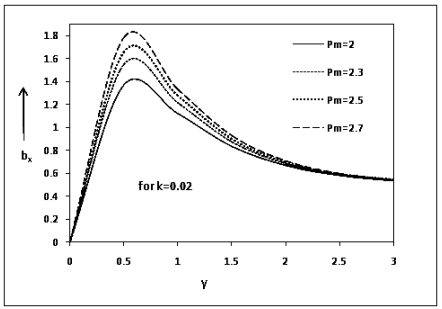

Figure 16
Induced Magnetic field b_x against y for M=2, Pr=2, Gr=5, Gm=5, Sc=1.5, R=1.5, H=0.5, U=1.

From the expression (40) and (41) it can be noted that the rate of heat transfer in terms of Nusselt number and the rate of mass transfer in terms of Sherwood number are not significantly affected by the visco-elastic parameter.

5. Conclusions

The present study gives a theoretical treatment about the effects of visco-elasticity on the steady mixed convective *MHD* flow past an infinite vertical porous plate with radiation and constant heat flux, taking into account the induced magnetic field and viscous dissipation. From the results the following conclusions could be drawn:

- The flow field is considerably affected by the visco-elastic parameter.
- The effect of visco-elasticity is maximum near the surface of the wall.
- Modification of visco-elastic parameter enhances the magnitude of shearing stress experienced by visco-elastic fluid in comparison with Newtonian fluid.
- Increasing values of Magnetic parameter, magnetic Prandtl number, radiation parameter and Schmidt number decline the speed of fluid flow. Also, the speed of fluid flow is enhanced on the cooled plate in comparison with flow past a heated plate.
- An increase in radiation parameter leads to amplify the temperature, while increasing Prandtl number decelerate the temperature.
- The induced magnetic field varies significantly with the magnetic parameter and magnetic Prandtl number for visco-elastic fluid.

References

1. Sakiadis, B.C. – Boundary layer behavior on continuous surfaces, American Institute of Chemical Engineers J. **7**, 26-28 (1961).
2. Bejan, A. and Khair, K.R. – Heat and mass transfer in a porous medium, Int. J. Heat Mass transfer, **28**, 902-918 (1985).
3. Pop, I. and Soundalgekar, V. M. – The unsteady free convection flow past an infinite plate with constant suction and heat sources, Int. J. Heat Mass transfer, **17**, 85-91 (1974).
4. Elbashbeshy, E.M.A. – Heat transfer over a stretching surface with variable heat flux. J. Physics D: Applied Physics, **31**, 1951-1955 (1998).
5. Cowling, T.G. – Magnetohydrodynamics, Interscience Publishers, New York (1957).
6. Sparrow, E.M. and Cess, R. D. – The effect of a magnetic field on free convection heat transfer, Int. J. Heat Mass Transfer, **3**, No.4, 267-274 (1961).
7. Riley, N. – Magneto-hydrodynamic free convection, J. Fluid Mechanics, **18,** No.4, 577-586 (1964).
8. Crammer, E.M. and Pai, S.I. – Magneto-fluid Dynamics for Engineering and Applied Physicists, McGraw-Hill, New York (1974).
9. Glauer,t M. B. – The boundary layer on a magnetized plate, J. Fluid Mechanics, **12**, No.4, 625-638 (1962) .
10. Raptis, A. and Soundalgekar, V. M. – MHD flow past a steadily moving infinite vertical porous plate with constant heat flux, Nuclear Engineering and Design, **72**, No.3, 373-379 (1982).
11. Raptis, A. and Kafousias, N. – Magneto hydrodynamics free Convective flow and mass transfer through a porous medium bounded by an infinite vertical porous plate with constant heat flux, Canadian J. Physics, **60**, 1725-1729 (1982).
12. Kafousias, N.G. and Georgantopoulos, G.A. – Magnetohydrodynamic free convection effects on the Stokes problem for an incompressible viscous fluid past an infinite vertical limiting surface, Astrophysics and Space Science, **85**, No.1-2, 297-307 (1982).
13. Raptis, A. and Soundalgekar, V. M. – MHD flow past a steadily moving infinite vertical porous plate with mass transfer and constant heat flux. ZAMM- J. Applied Mathematics and Mechanics, **64**, No.7, 789-812 (1982).
14. Acharya, M., Dash, G. C. and Singh, L. P. – Magnetic field effects on the free convection and mass transfer flow through porous medium with constant suction and constant heat flux. Indian J. Pure Applied. Mathematics, **31**, No.1, 1-18 (2000).

15. Singh, N.P., Singh, A.K. and Singh, A.K. – MHD free convention mass transfer flow part of flat plate, The Arabian J. for Science and Engineering, **32,** No.1A, 93-112 (2007).
16. Makinde, O.D. – On MHD boundary layer flow and mass transfer past a vertical plate in a porous medium with constant heat flux, Int. J. Numerical Methods for Heat and Fluid flow, **19**, No.3, 546-554 (2009).
17. Abdelkhalek, M. M. – Heat and mass transfer in MHD free convection from a moving permeable vertical surface by a perturbation technique, Communications in Nonlinear Science and Numerical Simulation, **14**, No. 5, 2091-2102 (2009).
18. Singh, N.P. and Singh, A. K. – MHD effects on Heat and mass transfer in flow of a viscous fluid with induced magnetic field, Int. J. Pure Applied. Physics, **38**, 182-189 (2000).
19. Ahmed, S. – Induced magnetic field with radiating fluid over a porous vertical plate: Analytical study, *J.* Naval Architecture and Marine Engineering, **7**, 83-94 (2010).
20. Ahmed, N., Sarma, D. and Deka, H. – MHD Mixed Convection and Mass Transfer from an infinite Vertical Porous Plate with Chemical Reaction in Presence of a Heat Source, Applied Mathematical Sciences, **6**, No. 21, 1011-1020 (2012).
21. Walters, K. – The solution of flow problems in the case of materials with memories, J. Mecanique, **1**, 473-478 (1962).
22. Choudhury, R. and Dey, B. – Flow features of a conducting visco-elastic fluid past a vertical permeable plate, Global journal of Pure and Applied mathematics, **13**, No. 9, 5687-5702 (2017).
23. Siddappa, B. and Abel, M. S. – Visco-Elastic Boundary Layer Flow past a Stretching Plate with Suction and Heat Transfer, Rheologica Acta, **25**, No. 3, 319- 320 (1986).
24. Subhas, M., Joshi, A. and Sonth, R. M. – Heat Transfer in MHD Visco-Elastic Fluid Flow over a Stretching Surface, Zeitschrift für Angewandte Mathematik und Mechanik, **81,** No.10, 691-698 (2001).
25. Sonth, R.M., Khan, S. K., Subhas, A. M. and Prasad, K. V. – Heat and Mass Transfer in a Visco-Elastic Fluid Flow over an Accelerating Surface with Heat Source/Sink and Viscous Dissipation, Heat and Mass Transfer, **38**, No.3, 213 -220 (2002).
26. Widodo, B., Siswono, G.O. and Imron, C. – visco-elastic fluid flow with presence of magnetic field past a porous circular cylinder, International Journal of mechanical and Production Engineering, **3**, No. 8, 123-126 (2015).

27. Choudhury, R. and Das, B. – Flow and heat transfer in MHD visco-elastic fluid with ohmic heating, Malaysian journal of Fundamental and Applied sciences, **12**, No.1, 47-57 (2016).

28. Abel, M. S., Sanjayanad, E. and Nandeppanavar, M. M. – Visco-elastic MHD flow and heat transfer over a stretching sheet with viscous and ohmic dissipations, Nonlinear science and Numerical Simulation, **13**, 1808-1821 (2008).

29. Choudhury, R., Bhattacharjee, H.K. and Dhar, P. – Visco-elastic flow with heat and mass transfer past a vertical porous plate in presence of hall current and radiation, Int. J. Fluids Engineering, **5**, No.1, 39-55 (2013).

30. Choudhury, R. and Das, B. – Influence of visco-elasticity on MHD heat and mass transfer flow through a porous medium bounded by an inclined surface with chemical reaction, International Journal of Heat and Technology, **34**, No. 2, 332-338 (2016).

INDIAN JOURNAL OF THEORETICAL PHYSICS, VOL. 66, NOS. 1 & 2, 2018

Development of a self controlled interferometer using optical Kerr medium as switching element

Agnijita Chatterjee[*] and Sourangshu Mukhopadhyay
Department of Physics, The University of Burdwan,
Burdwan-713104, West Bengal, India
[*]E-mail: agnijita.physics@gmail.com

[**Abstract:** Optical Kerr materials are very good choice for optical switching activities, optical self-focusing and defocusing and optical signal processing. The refractive index of optical Kerr medium depends on the intensity of light signal passing through such medium. Due to this said property Kerr medium can be used in phase conversion when light signal having time dependent intensity pattern is passed through the medium. If a saw-tooth type of intensity varying signal is passed through a Kerr medium, then a phase difference can be developed at output of the medium under specific conditions. Here in this paper the authors propose a new scheme of developing a self controlled interferometer using optical Kerr medium as switching element.]

Key words : Optical Kerr medium. Optical switching activities, Phase conversion, Self controlled interferometer.

1. Introduction

Optical Kerr materials are centro-symmetric nonlinear electro-optical materials. These materials play very significant role in optical signal processing, optical switching activities, optical self-focusing and defocusing etc[1-7]. These above mentioned applications can be possible only when a Kerr medium with very high nonlinear coefficient is triggered by an intense laser beam. Kerr material has a 2nd order nonlinearity in dielectric polarization and due to this nonlinearity the refractive index of Kerr medium depends on the intensity of light passing through the medium[8-16]. For this property Kerr medium can induce a phase difference between light signal passing directly through the medium and a part of the said signal after getting a feedback through the same medium. In this paper the authors propose a new scheme

of developing self controlled interferometer using optical Kerr medium as switching element.

2. Use of Kerr material for frequency variation of a light pulse

In a Kerr medium the refractive index (n) of the medium depends on the intensity (I) of light signal passing through the medium as

$$n = n_0 + n_2 I \quad \ldots \quad (1)$$

where, n_0 represents constant refractive index term and n_2 represents a nonlinear correction term. Due to this intensity dependent refractive index of the medium the propagation constant of a light beam in this medium also depends on the intensity (I) of light as

$$\beta = \beta_0 + K_0 n_2 I \quad \ldots \quad (2)$$

where, β_0 is the constant propagation factor and K_0 is the free space propagation constant of the light.

An incident electromagnetic wave having electric field $E = A \exp(i\omega_0 t)$ after passing through a Kerr medium of length 'l' would have electric field of the form

$$E_1 = A \exp[i(\omega_0 t - \beta l)]$$

Hence $$E_1 = A \exp[i(\omega_0 t - \beta_0 l - K_0 n_2 l I)]$$

where A represents amplitude and ω_0 represents frequency of the signal.

Therefore, the instantaneous frequency of output light signal becomes

$$\omega(t) = \omega_0 - K_0 n_2 l \, dI/dt \quad \ldots \quad (3)$$

Here, intensity I is a function of time t.

Thus, one can observe that Kerr medium can be used to convert the frequency of the light signal passing through the medium by the intensity variation of the light used.

3. Application of saw-tooth light pulse in Kerr material

In the previous section one can see that how Kerr medium can be used in frequency conversion when a light signal having time dependent intensity pattern is passed through such a medium[1-2]. Now, a saw-tooth light pulse is

considered as input signal to the Kerr medium. In a saw-tooth light pulse the intensity I of the pulse varies with time t as

$$I(t) = Kt \; ; 0 < t < T_0 \qquad \ldots \quad (4)$$

where, K=constant, at, $t = T_0$, $I = I_0$

So, $$K = I_0/T_0$$

Thus $I(t) = (I_0/T_0)\, t \; ; 0 < t < T_0$

The intensity variation with time for a saw-tooth light pulse is shown in Fig. 1.

Now, a saw-tooth light pulse is applied to the input of a Kerr medium. At the output of the medium one can get a output signal having electric field

$$E' = A \exp [i(\omega_0 t - \beta_0 l - K_0 n_2 l I_0/T_0 t)].$$

4. Self-controlled all-optical interferometer

A saw-tooth light pulse (Eq. 4) is applied to a Kerr medium as shown in Fig. 2. The electric field associated with the input saw-tooth light pulse is of the form

$$E = A \exp (i\omega_0 t)$$

At output half portion of output pulse is made feed back to the input of the same medium.

The electric field of the output signal passing directly through the medium is

$$E_1 = A/2 \exp [i(\omega_0 t - \beta_0 l - K_0 n_2 l I_0/T_0 t)] \qquad \ldots \quad (5)$$

The electric field associated with output signal after getting a feedback through the same medium is

$$E_2 = A/2 \exp [i(\omega_0 t - 2\beta l)]$$

Thus, $$E_2 = A/2 \exp [i(\omega_0 t - 2\beta_0 l - 2K_0 n_2 l I_0/T_0 t)] \qquad \ldots \quad (6)$$

It is clear from the expressions of electric field that a phase difference exists between these two output signals [Eq. (5) and Eq. (6)].

The phase difference is

$$\Delta\Phi = \omega_0 t - \beta_0 l - K_0 n_2 l I_0/T_0 t - \omega_0 t + 2\beta_0 l + 2K_0 n_2 l I_0/T_0 t$$

Therefore, $$\Delta\Phi = \beta_0 l + K_0 n_2 l I_0/T_0 t \quad \ldots \quad (7)$$

Phase difference can be controlled by I_0 and T_0 ratio.

5. Operational result

To calculate phase difference for *MO*/Polyimide material which has very high and negative value of nonlinear coefficient is taken into consideration[17].

$n_2 = -5.70\times10^{-6}\ cm^2/w$
$\lambda_0 = 488\times10^{-7}\ cm$
$l = 1\ cm$
$n_0 = 1.66$

By putting these values one can get phase difference from Eq. (5) as

$$\Delta\Phi = 2.12\times10^5 - 1.46\ I_0/T_0 t$$

Let, at, $t = t_1$, $\Delta\Phi = 0$ and at, $t = t_2$, $\Delta\Phi = \pi$

When $\Delta\Phi = 0$, one get a light at the output because of constructive interference and for $\Delta\Phi = \pi$ no light will come at the output because of destructive interference.

By putting these values of $\Delta\Phi$ and t one can get t_1 and t_2

$$t_1 = 145205.4794\ T_0/I_0$$

$$t_2 = 145203.3268\ T_0/I_0$$

Time difference becomes,

$$\Delta t = t_1 - t_2$$

Thus, $$\Delta t = 2.1526\ T_0/I_0$$

This is time (Δt) between constructive and destructive interferences.

To get $\Delta t = 1\mu s = 10^{-6}\ s$, the I_0 and T_0 ratio should be

$$I_0/T_0 = 2.1526\times10^6$$

The graphical representation of $\Delta\Phi$ with Δt is shown in Fig.3. Fig.3. shows that, if I_0/T_0 is fixed to a particular value that is $2.1526\times10^6\ W/cm^2 s$

then a self controlled interferometer can be developed with ON-OFF time interval of $1\mu s$. Whereas Fig.4 shows that with the change of I_0/T_0 value the ON-OFF pulse frequency (F) can be changed linearly. One can control the ON-OFF pulse frequency by choosing proper value of I_0 and T_0 ratio.

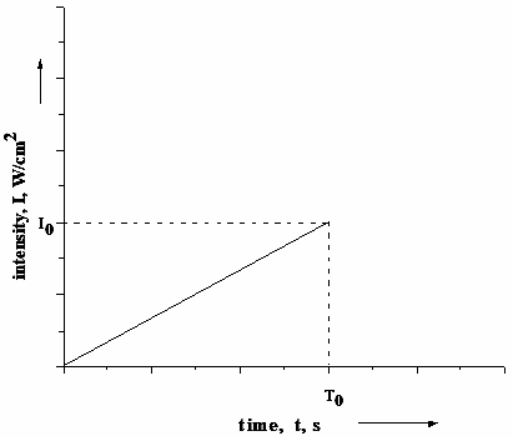

Figure. 1

Intensity variation with time for a Saw-tooth type of intensity varying signal.

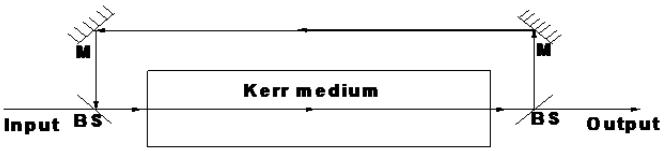

Figure. 2

The Kerr material based self controlled interferometer.

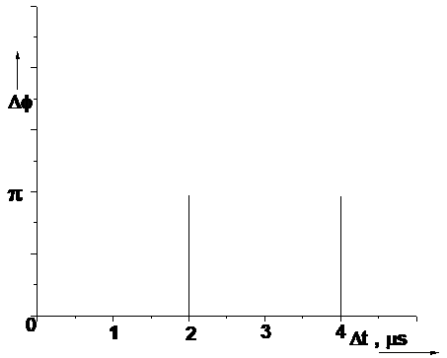

Figure. 3

Graphical representation of phase difference ($\Delta\Phi$) with Δt.

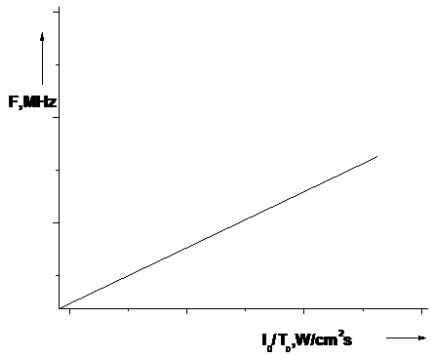

Figure. 4
Graphical variation of ON-OFF pulse frequency (F) with I_0 and T_0 ratio.

6. Conclusion

The non-linearity of optical Kerr medium leads to an intensity dependent phase difference between two light signals – one is directly passed through Kerr medium and another is passed through the same medium after getting a feed back. The whole method is all-optical one. By choosing proper value of I_0 and T_0 ratio the desired ON-OFF pulse frequency can be achieved. Therefore, Kerr medium can be used as switching element of an all-optical self-controlled interferometer. The proposed scheme is highly advantageous in optical communication especially in phase encoded signal processing. The scheme can lead also to many applications in fiber optic communication as one can get a desired ON-OFF pulse frequency by changing the slope of the saw-tooth curve. The temporal dispersion of light pulse is an important limitation in any type of optical communication. The proposed scheme is, in same way, goes under dispersion limitation. If the On-Off bits are sent through a single mode optical fiber the possibility of multimode dispersion is avoided completely, whereas the material and wave guide dispersion exist. As the proposed scheme uses a laser beam of high mono-chromaticity so the question of material and waveguide dispersion may be removed if the wavelength of the used light exhibits dispersion cancellation phenomenon in the optical fiber. For pure Silica made fiber this dispersion cancellation is found near about at 1330 *nm* wavelength. Hence if one selects this wavelength for communication of On-Off bits the question of dispersion

will be avoided totally for high bit rate communication beyond *GBPS*. Again the different types of nonlinearities (like Kerr type, stimulated Raman scattering type, four wave mixing type of nonlinearity etc.) may cause some frequency broadening or chirping, or splitting etc. As the proposed considers only On and Off (presence and absence) states of light, so the spectral change of light will not show any major effect during detection of the On-Off states at the output of the concerned optical fiber. This is a major advantage of the scheme. It is important to mention that the duration of the input saw-tooth pulse is selected in such a way that only one feedback of light is done, *i.e.* no second feedback is allowed. In optical fiber communication the proposed method may be useful to generate proper On-Off bit-rate using this all-optical scheme.

References

1. Chatterjee, A. and Mukhopadhyay, S. A. − New Method of Obtaining an Ultrashort Optical Pulse by the Use of Optical Kerr Material and a Sawtooth Optical Pulse, International Journal of Electronics & Communication Technology, **6**, Issue 1, 42-43, (2015).
2. Chatterjee, A., Biswas, A. and Mukhopadhyay, S. − Method of frequency conversion of Manchester encoded data from a Kerr type of nonlinear medium, J.Opt.,**46**, Issue 4, 415-419 (2017).
3. Xu, J., Yu, X., Lu, W., Qu, F. and Deng, N. − Offset Manchester coding for rayleigh noise suppression in carrier distributed WDM-POMS, Opt.Commun., **346**, 106-109, (2015).
4. Leuuthold, J. and Bres, C. S. − All-optical pulse shaping for highest spectral efficiency, Springer Ser. Opt. Sci., **194**, 217-260, (2015).
5. Cailean, A. M.,Cagneau, B. and Chassagne, L. − Evaluation of the noise effects on visible light communications using Manchester and Miller coding, Conference Proceedings, Development and Application System (DAS), IEEE, 85-89, (2014).doi: 10.1109/DAA-S.2014.6842433
6. Chakraborty, B. and Mukhopadhyay, S. − Alternative approach of conducting phase-modulated all optical logic gates, Opt. Eng., **48**, Issue. 3,035201, (2009).
7. Vitek, M. and Musevic, I. − Nanosecond control and optical pulse shaping by stimulated emission depletion in a liquid crystal, Opt. Express., **23**, Issue 13, 16921-16932, (2015).

8. Dhar, S. and Mukhopadhyay, S. − All optical implementation of ASCII by use of nonlinear material for optical encoding of necessary symbols, Opt.Eng., **44**, Issue **6**, 065201, (2005).

9. Samanta, D. and Mukhopadhyay, S. − All-optical method for maintaining a fixed intensity level of a light signal in optical computation, Opt. Commun., **281**, Issue 19, 4851-4853, (2008).

10. Chandra, S. K., Biswas, S. and Mukhopadhyay, S. − Phase encoded alloptical reconfigurable integrated multilogic unit using phase information processing of four wave mixing in semiconductor optical amplifier, IET Optoelectronics., **10**, Issue 1, 1-6, (2016).

11. Sen, S. and Mukhopadhyay, S. − Reduction of VP voltage of an electro-optic modulator by the oblique end cutting and multi-rotation, Opt. Laser Technol., Elsevier, **59**, 19-23, (2014).

12. Bhattacharya, S., Patra, S.N. and Mukhopadhyay, S. − An all optical prototype neuron based on optical Kerr material, Optik-International Journal for Light and Electron Optics., **126**, Issue 1, 13-18, (2015).

13. Robles, F.E., Fischer, M.C. and Warren,W.S. − Femtosecond pulse shaping enables detection of optical Kerr-effect (OKE) dynamics for molecular imaging, Opt. Lett., **39**, Issue 16, 4788-4991, (2014).

14. Biswas, S. and Mukhopadhyay, S. − All-Optical approach for conversion of a binary number having a fractional part to its decimal equivalent to three places of decimal using single system optical tree architecture, J. Opt., **43**, Issue 2, 122-129, (2014).

15. Liu,Y., Qin, F., Zhou, F., Meng, Q-b., Zhang, D-z. and Li, Z-y. − Ultrafast optical switching in Kerr nonlinear photonic crystals, Front. Phys. China., **Vol. 5**, Issue 3, 220-244, (2010). doi: 10. 1007/s11467-010-0100-0

16. Li, Z-Y. and Meng, Z-M. − Polystyrene Kerr nonlinear photonic crystals for building ultrafast optical switching and logic devices, J. Mater. Chem., C **Vol. 2**, Issue 5, 773-954, (2014).

17. Lukasz, Brzozowski and Sargent Edward, H. − Azobenzenes for photonic network applications: Third-order nonlinear optical properties, Journal of Materials Science: Materials in Electronics, **Vol. 12**, Issue 9, 483-489, (2001).

INDIAN JOURNAL OF THEORETICAL PHYSICS, VOL. 66, NOS. 1 & 2, 2018

Numerical analysis of hetrostructure semiconductor devices

Mukesh Kumar, Archana Kumari
University Department of Electronics, B.R.A. Bihar University
Muzaffarpur -842001, Bihar, India
E-mail : mukeshkumar4525@gmail.com,

Bidyanand Mahto
Department of Physics, Katihar Engineering College, Katihar
E-mail : bidyanandmadhuri@gmail.com

and

Tarun Kumar Dey
Post Graduate Department of Physics, L.S. College,
Muzaffarpur-842001, Bihar, India
E-mail : tkdeyphy@gmail.com

[**Abstract:** A numerical method for analyzing hetero structure semiconductor devices like transistor is described. The macroscopic semiconductor equations for materials with position-dependent dielectric constant, band gap, and densities of states are first cast into a form identical to that commonly used to model heavily doped semiconductors. Fermi-Dirac statistics are also included within this simple, Boltzmann like formulation. Because of the similarity in formulation to that employed for heavily doped semiconductors, well developed numerical techniques can be directly applied to hetero-structure simulation .A simple one-dimensional, finite difference solution is presented. The accuracy of the numerical method is assessed by comparing numerical results with special-case, analytical solutions.]

Keywords :Numerical method, hetero structure, simulation

1. Introduction

Hetero structure semiconductor devices show promise for use in high-performance integrated circuits; with the advent of new fabrication technologies, this well-known potential is being realized[1,2]. The design

flexibility possible with hetero structures has been used to improve the performance of bipolar transistors[2] and to realize new devices such as the modulation-doped field-effect, transistor (*MODFET*) which has already achieved a switching speed of less than 20 ps[3,4]**.** To aid in understanding the physical operation of these devices and to optimize their design, numerical hetero structure device models are required.

2. Applications

In this paper we discuss some examples of numerical analysis of hetero structures. Two devices, the hetero structure bipolar transistor and the two-dimensional electron gas (2*DEG*) *MESFET*, are considered. In the examples that follow, we adjusted the value of χ for Al_xGa_{1-X}. As to provide discontinuities in agreement with the Dingle rule[5].There combination mechanism assumed is Shockley-Read-Hall recombination[6] with the trap energy level located at the intrinsic level. Auger recombination, radiative recombination, and explicit generation mechanisms are not considered.

The computed equilibrium energy band diagram for an n^+ *GaAs/n GaAs/n GaAlAs/*p^+ *GaAs/n GaAs/*n^+ *GaAs HBT* is shown in Fig.1.

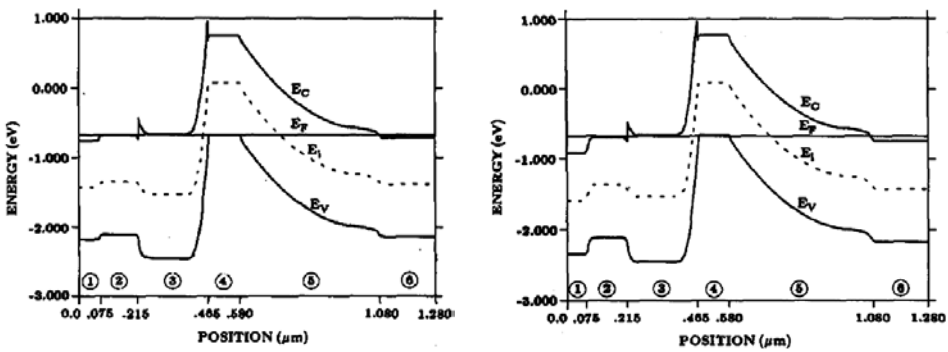

(*a*) (*b*)

Fig. 1

Equilibrium energy band diagrams for a hetero structure bipolar transistor. Figure 1(*a*) assumes Boltzmann statistics and Figure 1(*b*) Fermi-Dirac statistics.

Table 1 provides the details of this *HBT* which is similar to one described by Asbeck et al.[7]. Two cases, Boltzmann statistics (Fig. 1(*a*)) and Fermi-Dirac statistics (Fig. 1(*b*)) are considered. The increased penetration of the Fermi level into the conduction band of the heavily doped n^+ regions is readily apparent. Another important difference between the two cases is the slight lowering of the barrier height for the *n GaAs/n GaAlAs* junction caused by carrier degeneracy (an effect discussed by Kroemer[8]).

Table 1

HJBT device structure.

Layer	*ND-NA* (*cm*-3)	*Al* fraction	Thickness (μm)
1	1×10^{19}	0	0.075
2	5×10^{17}	0	0.125
3	5×10^{17}	0.30	0.25
4	-1×10^{19}	0	0.10
5	1×10^{16}	0	0.5
6	2×10^{18}	0	0.2

We now consider the injection characteristics of the *HJBT*'s emitter-base junction. The material parameters used for these calculations are displayed in Table 2**.** The bandgaps, effective masses, dielectric constants, and electron affinities for *GaAs* and *AlAs* are those given by Casey and Panish[9]. The corresponding parameters for $Al_{0.3}Ga_{0.7}As$ were obtained by the methods described by Sutherland and Hauser[10]. The minority-carrier lifetimes are typical of those obtained in *GaAs* solar cells[11]. Mobilities for *GaAs* are from[6] and for electrons in *AlGaAs* from String fellow[12]. The hole mobility of *AlGaAs* was set to its value in correspondingly doped *GaAs*[6]. For the base contact, we assumed a surface recombination velocity of

Table 2

Material parameters for the emitter-base junction.

Material Parameter	Emitter	Base
All fraction	0.30	0.0.
N_D-N_A	5×10^{17} cm^{-3}	1×10^{19} cm^{-3}
τ_n, τ_p	10^{-9} *sec*	10^{-9} sec
μ_n	2000 cm^2/V-*sec*	1200 cm^2/*V-sec*
μ_p	200 cm^2 / *V-sec*	100 cm^2 / *V-sec*
E_G	1.798	1.424
m_p^*	0.52 m_0	0.48 m_0
m_n^*	0.080 m_0	0.067 m_0
χ	3.75	4.07
k_S	12.0	13.1

of 5×10^6 *cm/s* to simulate the drift of carriers through the collector base space-charge region at the saturated velocity. The computed forward biased current (assuming Boltzmann statistics) showed an ideality factor of 1.05 for biases above 0.8 *V* where recombination within the space-charge region was not dominant.

The computed energy band diagram of the 1.0-*V* for-ward-biased emitter-base junction shown in Fig. 2 reveals a large change in the electron quasi-Fermi level across the space-charge region. This effect, caused by the spike in the conduction band, suppresses current injection and reduces the gain of an *HBT*[2]. The operation of this hetero junction was further investigated by numerical experiments. When the base contact was made ohmic, lthe diode current at 1*V* ($1.57 \times 10^{-4} A/cm^2$) increased by less than one percent. Similarly, when the base length was increased by a factor of 100, (from ~ 0.05 to ~ 5 minority-carrier diffusion lengths) the diode current was reduced by less than 15 percent. Since the base width is only 0.1 μm, the validity of a drift-diffusion description within the base is doubtful[13], but the numerical

experiments demonstrate that the diode current is not dominated by minority-carrier transport through the narrow quasi-neutral base region.

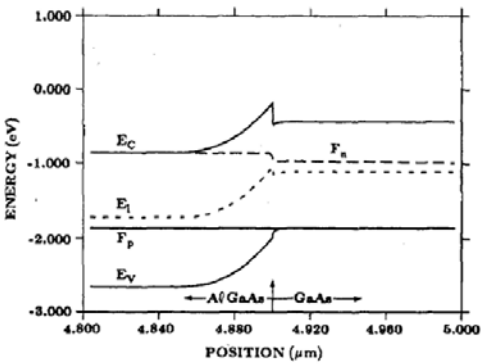

Fig. 2
AlGaAs : *GaAs* abrupt *n-p* hetero- junction under 1.0-*V* forward bias (only the region near the junction is shown).

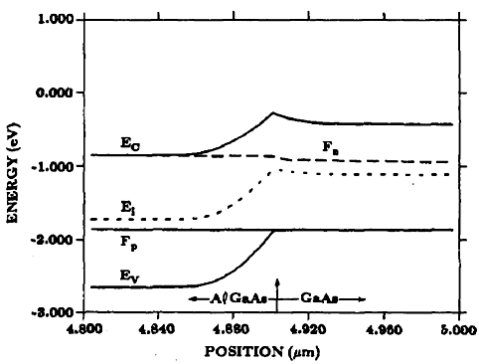

Fig. 3
AlGaAs graded *n-p* hetero- junction under 1.0-*V* forward bias.

Table 3

Material parameters for the 2*d* electron *GaAs* devices.

Material Parameter	Layer	
	GaAs	*GaAlAs*
Al Fraction	-	0.17
N_D	$1 \times 10^{16}\ cm^{-3}$	$2.6 \times 10^{17}\ cm^{-3}$
E_G	1.424	1.64
m_p^*	$0.48\ m_0$	$0.49\ m_0$
m_n^*	$0.067\ m_0$	$0.074\ m_0$
χ	4.07	3.89
k_S	13.1	12.5

The computed equilibrium electron density for this device is plotted in Fig. 4. As expected, the results show the depletion of electrons near the surface and on the *AlGaAs* side of the hetero junction and a strong accumulation layer of electrons on the *GaAs* side of the junction. To modulate the electron density in the accumulation layer (and, therefore, the conductance of the *FET*) a reverse bias is applied to the gate. The increasing penetration of the gate-controlled electric field for increasing reverse bias is illustrated in Fig. 5. As shown, the surface depletion layer expands rapidly

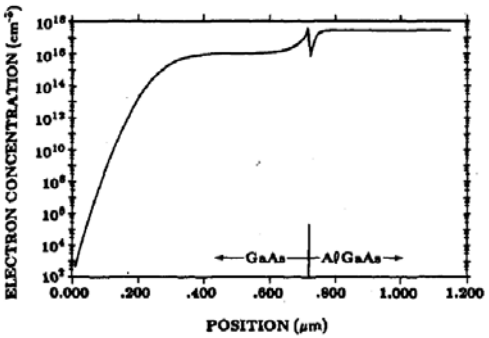

Fig. 4
Equilibrium electron concentration in the 2*DEG* structure.

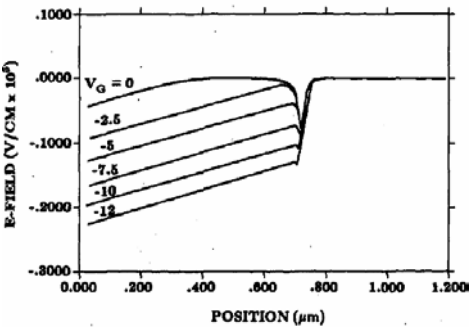

Fig. 5
Electric field versus position in the 2*DEG* structure.The identifying numbers on the curves refer to the bias applied between the gate and substrate.

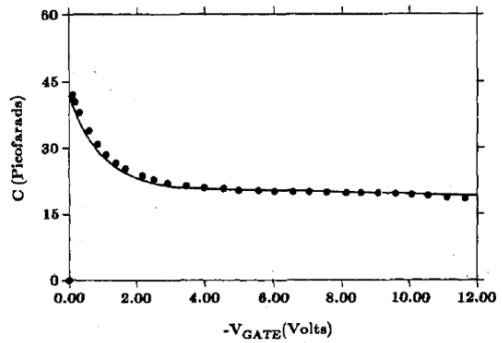

Fig. 6
Capacitance versus reverse gate voltage for the 2*DEG* structure. The data points are from[3].

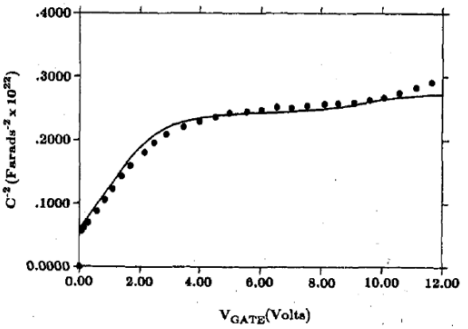

Fig. 7
Inverse capacitance squared versus gate voltage. The data points are from[3].

with reverse bias until the accumulation layer is encountered (at V_G ~ -2.5 *V*). Further bias simply decreases the electron concentration in

the accumulation layer without further penetration of the gate-controlled electric field. Finally, the accumulation layer is removed (at $V_G \sim -10V$) and additional reverse bias depletes the *AlGaAs* substrate. As Fig. 6 shows, the computed quasistatic capacitance agrees well with the reported characteristics[3]. The inverse capacitance squared plot in Fig. 7 shows the expected linear region while the top (*GaAs*) layer is being depleted and also when the *AlGaAs* substrate depletes. The computed results shows excellent agreement with the measured characteristics except at high bias where break-down may be occurring. For structures showing more pronounced quantum confinement of electrons at the hetero junction, the two-dimensional nature of the electron gas should be considered[5].

3. Conclusions

In this paper, a convenient formulation of the basic semiconductor equations for hetero structure device analysis was presented, discussed, and illustrated. The device equations for parabolic band semiconductors were reviewed and the similarity to the heavily doped semiconductor stressed. Two simplifying assumptions not valid in general, however, are usually made when modeling heavily doped devices. Specifically, the total band change V_G, is arbitrarily split into its components V_p and V_n and the spatial variation of the dielectric constant is ignored. Conventional device analysis codes, both one-and two-dimensional, are readily converted to hetero structure device simulation when these two simplifying assumptions are removed.

A significant advantage of the formulation presented here is that it is a unified method for modeling both heavily doped silicon and hetero structure devices. In the past, different formulations have been used for these two problems[6,8,10]. Also important is the technique for including Fermi-Dirac statistics. The method presented retains the simple, widely used Boltzmanm-like formulation by incorporating additional drift-like terms in the carrier transport equations. This technique for incorporating Fermi-Dirac statistics is applicable for both homo structure and hetero structure devices.

Finally, some cautions regarding the classical formulation are in order. Our formulation of the semiconductor equations assumes a slow variation in material composition[14,15]. While such an assumption may be valid for intentionally graded junctions, it is obviously violated for abrupt hetero junctions. At an abrupt junction, quantum mechanical reflection and tunneling may be important[1] and should be included. Since hetero structure

devices are likely to be small, high-field and transient carrier transport will also occur[13] .

References

1. Milnes, A. G. and Feuct, D. L. − Heterojunctions and Metal semiconductor Junctions. New York: Academic Press (1972).
2. Kroemer, H. − "Heterostructure bipolar transistor and integrated circuits," Proc. IEEE, **Vol. 70,** 13-25 (1982).
3. Delagebeaudeuf, D., Delescluse, P., Etienne, P., Laviron, M., Chaplant, 1. and Linh, N. T. − "Two-dimensional electron gas MESFET structure," Electron. Lett., **16,** 667-668 (1980).
4. Gallagher, R. T. − "GaAs chip sets speed record at room temperature,'' Electronics, 81-82, Dec. 15 (1981).
5. Asbeck, P. M., Miller, D. L., Milano, R. A., Harris, J. S., Jr. Kaelin, G. R. and Zucca, R. "(Ga,Al)As/GaAs bipolar transistors for digital integrated circuits," in IEDM Tech. Dig., 629-632 (198l).
6. Sze, S**.** M. − Physics of Semiconductor Devices, 2nd ed., New York: Wiley,(1982).
7. Casey, H. C. Jr. and Panish, M. B. – Hetero structure Lasers. New York:Academic Press, (1978).
8. Kroemer, H. − "Analytic approximations for degenerate accumulation layers in semiconductors with applications to barrier lowering in isotype heterojunctions," J. Appl**.** Phys., **52,** 873-878 (1981).
9. Sekela, A. M., Feucht, D. L. and Milner, A. G. − "Efficiency calculations for heteroface solar cells," IEEE Trans. Electron Devices, **ED-24,** 373-380 (1977).
10. Sutherland, J. E. and Hauser, J. R. − "A computer analysis of heterojunction and graded composition solar cells," IEEE Trans. Electron Devices, Vol. ED-**24,** 363-372 (1972).
11. Stringfellow, G. B. − "Electron mobility in Al, Ga,-,As," J. Appl. Phys., **50,** 4178-4183 (1979).
12. Baccarani, G., Jacaboni, C. and Mazzone, A. M. − "Current transport in narrow-base transistors," Solid-State Electron., **20**, pp. 5-10 (1977).
13. Kressel, H**.** and Butler, J. K. − Semiconductor Lasers and Heterojunction LEDs. New York: Academic Press (1973).
14. Aymerich, X. - Humet, Serra, F. -Mestres, and Millan, J. − "An analytical approximation for the Fermi-Dirac integral F3"*q,)*/,," (Solid-state Electron, **24**, 981-982 (1981).
15. Beer, A. C., Chase, M. N. and Choquard, P. F. − "Extension of McDougall-Stones tables of the Fermi-Dirac functions," H eh. Phy**.** Acta., **28,** 529 (1955).

INDIAN JOURNAL OF THEORETICAL PHYSICS, VOL. 66, NOS. 1 & 2, 2018

Analysis of memory and self affinity and identification of governing process in solar flare index signal

Shankhachur Mukherjee
Department of Physics, The University of Burdwan,
Golapbag, Burdwan-713104, India
E-mail: ahlechaos@gmail.com

Kausik Rakshit
Department of Basic Science, Regent Education and Research Foundation,
Barrackpore, Kolkata-700121, India
E-mail: kausik6726@gmail.com

and

Koushik Ghosh
Department of Mathematics, University Institute of Technology,
The University of Burdwan, Golapbag (North),
Burdwan-713104, India
E-mail: koushikg123@yahoo.co.uk

[Abstract: A solar flare is a sudden brightening observed over the sun's surface or the solar limb which is interpreted as energy release of large amount up to the order of 6×10^{25} Joules of energy (about one sixth of the total energy output of the sun per second). It is an eruption of magnetic energy released on or near the surface of the sun, usually associated with sunspots, accompanied by bursts of electromagnetic radiation and particles. Solar flares strongly influence the local space weather in the vicinity of the Earth. They can produce stream of highly energetic particles in the solar wind, known as a solar proton event or "coronal mass ejection" (*CME*). These can impact the Earth's magnetosphere and present radiation hazards to spacecraft, astronauts and cosmonauts. In the present paper we have analyzed the solar flare index developed at Mc-Math-Hulbert Solar Observatory on daily basis during 1st January, (1966) to 31st December, (2008). The scaling analysis has been performed in the present data to understand the memory in the present signal. For the current study Finite Variance Scaling Method (*FVSM*) has been used after minimizing the trend in the original signal by Double Exponential Smoothing. *FVSM* method gives fractional variation and indicates an anti-persistent memory of the present solar flare index signal. We have employed Higuchi method for calculating the fractal dimension which

indicates that the governing process is self similar. In addition to this we have gone through the process of Yule –Walker to identify whether the present signal is governed by autoregressive process or not. The present study clearly indicates that the present solar flare index signal is governed by an autoregressive method of short order. In fine the entire analysis possibly suggests that sudden eruption of magnetic energy released on or near the surface of the Sun is a self affine short memory process governed by an autoregressive method.]

Keywords: Solar Flare index, Double Exponential Smoothing, Finite Variance Scaling Method, Higuchi Method, Yule –Walker Method, Autoregressive Process.

1. Introduction

Solar Flares are rapid intense variation in brightness of the sun. It is widely accepted that they are the result of the rapid conversion of a large amount of magnetic energy, previously stored in the solar corona, and dissipated through magnetic reconnections. In the Sun, magnetic reconnection may occur on a series of closely happening loops of magnetic lines of force. These lines of force sharply reconnect into a low arcade of loops exposing a helix of magnetic field unconnected to the rest of the arcade. The unconnected magnetic helical field and the material that it includes may viciously inflate outwards generating a coronal mass ejection[1]. The release of energy takes place in a matter of minutes to hours, and can amount to values up to 10^{33} *erg*. The resulted electromagnetic radiation can extend over a very broad range of wavelengths, from gamma rays and *X*-rays at the shortest wavelengths to radio waves at the long-wavelength end of the spectrum. The energy released heats the surrounding plasma to temperatures that can be as high as 50×10^{9} *K*, representing the highest temperatures that plasma can reach in the solar atmosphere. It is now well known that flares act as very efficient particle accelerators. Through the electric fields associated with the varying magnetic fields that are characteristic for such magnetically complex active regions, electrons and ions could be accelerated to energies up to 100 *MeV*.

Double Exponential Smoothing[2,3,4] is an effective prescription to efface noise from a signal. The essence of this method lies in the fact that whenever a signal bears any kind of trend, which is a sort of lingering effect

associated with a signal, this method works well to de-trend it for further analysis.

Fractal method has been studied to understand the irregular and chaotic nature of graphical structure. Since fractals were introduced in physics, their applications promoted enormous progress in understanding phenomena that are most directly involved in formation of irregular structures. A broad class of clustering phenomena such as filtration, electrolysis and aggregation of colloids and aerosols has received a good deal of attention. Other phenomena that are not strictly clustering effects (*i.e.*, dielectric breakdown, formation of a contact surface when two liquids are mixed etc.) can be advantageously treated using fractals. Describing natural objects by geometry is as old as science itself; traditionally this has involved the use of Euclidean lines, rectangles, cuboids, spheres and so on. But, nature is not restricted to Euclidean shapes. Mandelbrot[5] observed that "clouds are not spheres, mountains are not cones, coastlines are not circles, bark is not smooth, nor does lightning travel in a straight line". Most of the natural objects we see around us are so complex in shape as to deserve being called geometrically chaotic. They appear impossible to describe mathematically and used to be regarded as the "monsters of mathematics". Mandelbrot[5] introduced the concept of fractal geometry to characterize these monsters quantitatively and to help us to appreciate their underlying regularity. The simplest way to construct a fractal is to repeat a given operation over and over again deterministically. The classical Cantor set is a simple text book example of such a fractal. It is created by dividing a line into n equal pieces and removing $(n-m)$ of the parts created and repeating the process with m remaining pieces ad infinitum. However, fractals that occur in nature occur through continuous kinetic or random processes. Having realized this simple law of nature, we can imagine selecting a line randomly at a given rate, and dividing it randomly, for example. We can further tune the model to determine how random this randomness is. Starting with an infinitely long line we obtain an infinite number of points whose separations are determined by the initial line and the degree of randomness with which intervals were selected. The properties of these

points appear to be statistically self-similar and characterized by the fractal dimension, which is found to increase with the degree of increasing order and reaches its maximum value in the perfectly ordered pattern. It is now accepted that when the power spectrum of an irregular discrete signal is expressed by a single power law $F^{-\alpha}$ (where F stands for frequency) the discrete signal shows a property of a fractal curve[6]. As the fractal length $L(k)$ of the discrete signal is expressed as $L(k) \propto k^{-D}$, where k is the time interval, the fractal dimension D is expected to be closely related to the power law index[6,7] α. Higuchi[6,7] developed a new method for calculating the fractal dimension of a given discrete signal and the relation between α and D has been investigated by him[6,7] as $D = \frac{(5-\alpha)}{2}$.

In the present work we have taken into consideration the daily solar flare index data developed at McMath-Hulbert Solar Observatory during 01 January, (1966) - 31 December, (2008) (covering four solar cycles solar cycle 20-23) (website : ftp://ftp.ngdc.noaa.gov/STP/SOLAR_DATA/SOLAR_FLARES/FLARES_INDEX/DAILY.PLT).

We can observe conspicuous trend in the present signal. To minimize this trend we have employed Double Exponential Smoothing[2,3,4] in it. To understand the memory in the present signal we have used Finite Variance Scaling Method (*FVSM*)[8,9,10] to understand the memory in the present signal. We have further employed Higuchi method[6,7] on the smoothed signal to calculate the fractal dimension which gives fractal nature of the signal. In addition to this we have gone through the process of Yule-Walker[11,12,13] to identify whether the present signal is governed by autoregressive process or not.

2. Theory

2.1 Smoothing of Signal: Double Exponential Smoothing :

The Double Exponential Smoothing or Second Order Exponential Smoothing was first developed by Brown[2] and later modified by Holt[3] and Winters[4] to effectively remove trends from a given signal which basically distorts the relationship of one's interest. The method of Double

Exponential Smoothing[2,3,4] is governed by the following system of equations shown below :

and

$$\left.\begin{aligned} x_1^{(p)} &= x_1 \;;\; b_1 = x_2 - x_1 \\ x_i^{(p)} &= \alpha x_i + (1-\alpha)(x_{i-1}^{(p)} + b_{i-1}) \\ b_i &= \beta\,(x_i^{(p)} - x_{i-1}^{(p)}) + (1-\beta) b_{i-1} \\ & \qquad (i = 2,3,4,\ldots..,N) \end{aligned}\right\} \quad \ldots \quad (1)$$

where $\{x_i\}_{i=1}^{N}$ is the observed discrete signal, $\left\{x_i^{(p)}\right\}_{i=1}^{N}$ is the smoothed signal and $\{b_i\}_{i=1}^{N}$ is the trend traced in the signal, α and β are the 'signal smoothing parameter' and 'trend smoothing parameter' respectively. We have $0 < \alpha < 1$ and $0 < \beta < 1$.

2.2 Estimation of Hurst Exponent using Finite Variance Scaling Method (FVSM) :

For the scaling analysis of a given discrete time-dependent signal Finite Variance Scaling Method (*FVSM*) is a very useful technique[8,9,10]. A well-known version of *FVSM* is the Standard Deviation Analysis (*SDA*)[10]. For a given time dependent finite discrete signal $x(t_i)$ (where i=1, 2,…. , N) this method gives rise to a sequence of cumulative standard deviations $D(t_j)$ associated with the partial signals $\{x(t_i)\}(i=1, 2,\ldots. , j)$ (where j=1, 2,...., N) by the following manner :

$$D(t_j) = [\tfrac{1}{j}\textstyle\sum_{i=1}^{j} x^2(t_i) - \{\tfrac{1}{j}\sum_{i=1}^{j} x(t_i)\}^2]^{\frac{1}{2}}, \text{ for } j=1,2,3....,N \quad \ldots \quad (2)$$

For self similar signals eventually we can find that this $D(t)$ follows a power law by the following way : [8,9,10]

$$D(t) \propto t^H \quad \ldots \quad (3)$$

Here H is the Hurst Exponent and it can be estimated from the slope of the best fitted straight line in the plot of log $D(t)$ versus log (t).

The value of the Hurst exponent ranges between 0 and 1. The limiting case H=0, corresponds to white noise, where fluctuations at all frequencies

are equally present. A Hurst exponent value $0<H<0.5$ will exist for a signal with anti-persistent behaviour. In this case the signal is governed by a short memory process. A value of 0.5 indicates a true random walk (a Brownian signal). In a random walk there is no correlation between any element and future element. If we have $0.5<H<1.0$, the process is present with persistent behaviour. A Hurst Exponent value in this range indicates a long memory process.

2.3 Determining the Fractal Dimension of a Self Similar Signal (Higuchi Method):

Higuchi[6,7] developed a method for calculating the fractal dimension of a given self similar signal. His method is as follows.

We take a finite set of signal taken at a regular interval:

$$X(1), X(2), X(3),\ldots, X(N).$$

From the given signal, we construct a new signal $\{X(m), X(m+k), X(m+2k), \ldots, X(m + [(N - m) / k] . k)\}$where [ ] denotes the greatest integer function and both k and m ($m = 1, 2, 3, \ldots, k$) are integers, m and k indicate the initial time and the interval time respectively. Then k sets of new signal are obtained. We define the length of the curve of the new signal as follows :

$$L_m(k) = \{(\sum_{i=1}^{\left[\frac{N-m}{k}\right]} |X(m+ik) - X(m+(i-1)k)|) \frac{N-1}{\left[\frac{N-m}{k}\right].k} / k \quad \ldots \quad (4)$$

The length of the curve for the time interval k, $\langle L(k)\rangle$ is defined as the average value over k sets of $L_m(k)$. If $\langle L(k)\rangle \propto k^{-D}$, we judge the curve is fractal with dimension D. We deduce fractal dimension D from the slope of the best fitted line corresponding to the plot of $\log\langle L(k)\rangle$ against $\log k$.

We can determine the randomness of a signal by determining fractal dimensions and from this we can conclude whether a physical structure is perturbed (*i.e.* not in steady state) in nature or not. For any self affine

physical structure exhibited over a plane if the observed *D* lies between 1 and 2 then we can conclude that the structure is fractal in nature. For the ideal case of chaotic physical structure *D* is 5/3.

2.4 Determination of Autoregressiveness of a Signal by Yule –Walker Method :

We consider a discrete signal $\{x_i\}$; 1, 2, …., *N* observed at equally spaced time instants $t=\tau,2\tau,....,N\tau$ where τ is the uniform interval between any two consecutive observation instants. The time series is said to be governed by an autoregressive process of order *p* or in short *AR* (*p*) if we have[13]

$$\bar{x}_n = \sum_{i=1}^{p} \emptyset_i \bar{x}_{n-i} + \epsilon_n \qquad \ldots \quad (5)$$

where $n = p+1, p+2, \ldots, N$ and ε_n's ($n= p+1, p+2,.....,N$) are the noises which may be regarded as a whole as sequence of shocks driving the system; $\bar{x}_n = x_n - \mu$ for n=1,2,…,*N* which is the deviation of the process from the mean $\mu = \frac{1}{N}\sum_{i=1}^{N} x_i$ and ϕ_i's (i=1,2,……,p) are the process parameters. If further the noises are with mean very near to zero, *i.e.* $\frac{1}{N-p}\sum_{i=p+1}^{N} \epsilon_i \approx 0$. and with a low variance and uncorrelated then these are supposed to be white noise.

Yule[11] and Walker[12] developed a system of linear equations using the auto correlation functions $\rho_1, \rho_2, \rho_3, \ldots\ldots, \rho_{N-1}$ [lags 1 to (*N*-1)] for a given finite discrete signal $\{x_i\}_{i=1}^{N}$. The system of equations is given below :

$$\left.\begin{aligned}
\rho_1 &= \Phi_1 + \Phi_2\,\rho_1 + \Phi_3\,\rho_2 + \ldots\ldots + \Phi_N\,\rho_{N-1} \\
\rho_2 &= \Phi_1\,\rho_1 + \Phi_2 + \Phi_3\,\rho_1 + \ldots\ldots + \Phi_N\,\rho_{N-2}, \\
\rho_3 &= \Phi_1\,\rho_2 + \Phi_2\,\rho_1 + \Phi_3 + \ldots\ldots + \Phi_N\,\rho_{N-3} \\
\rho_{N-1} &= \Phi_1\rho_{N-1} + \Phi_2\rho_{N-2} + \Phi_3\rho_{N-3} + \ldots\ldots + \Phi_N
\end{aligned}\right\} \quad \ldots \quad (6)$$

We now consider $R = \begin{pmatrix} \rho 1 \\ \rho 2 \\ \vdots \\ \rho N \end{pmatrix}$ H= $\begin{pmatrix} \Phi 1 \\ \Phi 2 \\ \vdots \\ \Phi N \end{pmatrix}$

$$P = \begin{pmatrix} 1 & \rho 1 & \rho 2 & \rho 3 & \cdots & \rho N-1 \\ \rho 1 & 1 & \rho 1 & \rho 2 & \cdots & \rho N-2 \\ \rho 2 & \rho 1 & 1 & \rho 1 & \cdots & \rho N-3 \\ \rho 3 & \rho 2 & \rho 1 & 1 & \cdots & \rho N-4 \\ \vdots & \vdots & \vdots & \vdots & \ddots & \vdots \\ \rho N-1 & \rho N-2 & \rho N-3 & \rho N-4 & \cdots & 1 \end{pmatrix} \quad \ldots \quad (7)$$

So, we can have, $R=PH$ *i.e.*

$$H=P^{-1}R \quad \ldots \quad (8)$$

provided P is non-singular *i.e.* det $(P) \neq 0$.

By this Yule-walker equation[11,12,13] we can find the value of Φ_1, Φ_2, Φ_3, ……, Φ_N. Now the magnitudes are minutely observed coming for this parameters as a solution of the equation. Rationally to say, the signal will be considered as an autoregressive signal of order p if we have[13]

$$\left.\begin{aligned} \Phi_i \neq 0;\ 1 \leq i \leq p \\ =0;\ p \leq i \leq N \end{aligned}\right\} \quad \ldots (9)$$

Here, $\Phi_i = 0$ for $p \leq i \leq N$ practically means they lie in the neighbourhood of 0 compared to the Φ_i's for $1 \leq i \leq p$.

The matrix P is said to be the Yule-walker matrix[11,12,13]. If for a given signal the Yule-walker matrix appears to be positive definite the corresponding signal is considered to be a stationary signal.

3. Results

In the present work for Double Exponential Smoothing the values of α and β are taken as 0.68 and 0.74 respectively in order to maintain the positional importance[14]. The original Solar Flare Index signal and the corresponding smoothed signal are demonstrated by the following graphical illustrations as shown below :

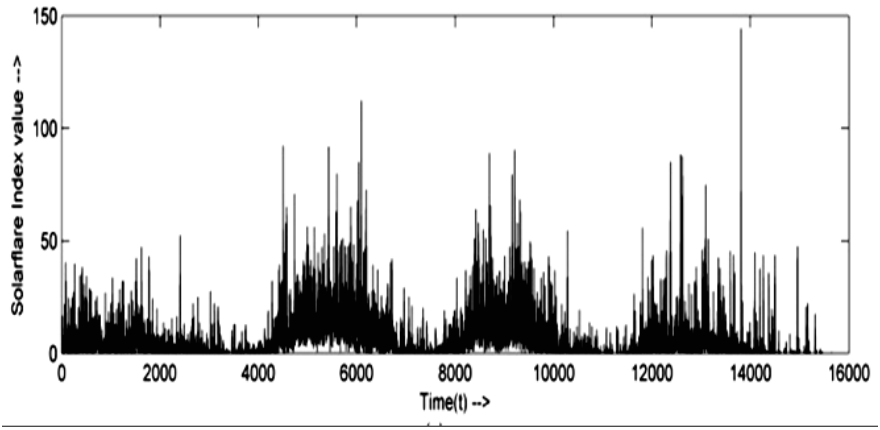

(*a*)

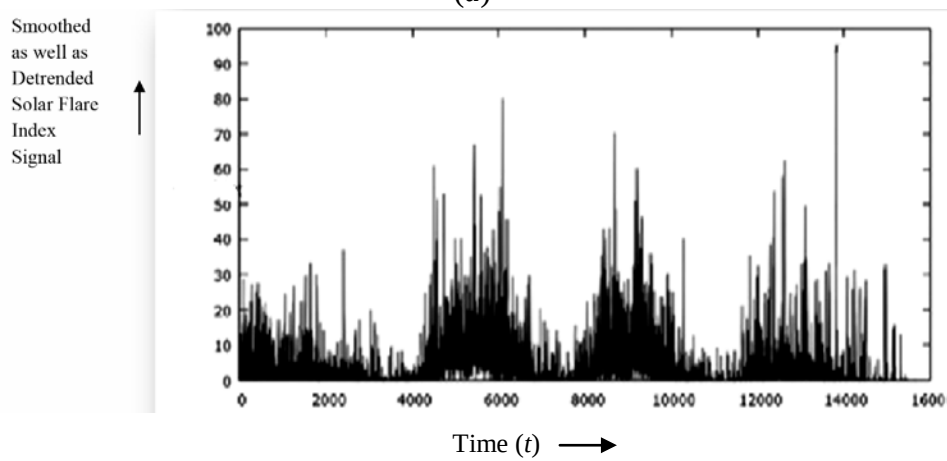

(*b*)

Figure 1
(*a*) Original and (*b*) Smoothed as well as De-trended Solar Flare Index Signal by Double Exponential Smoothing.

Next *FVSM* has been applied on the present smoothed signal and the calculation yields the value of *H* as 0.1316 which confirms that the present signal is governed by a short memory process.

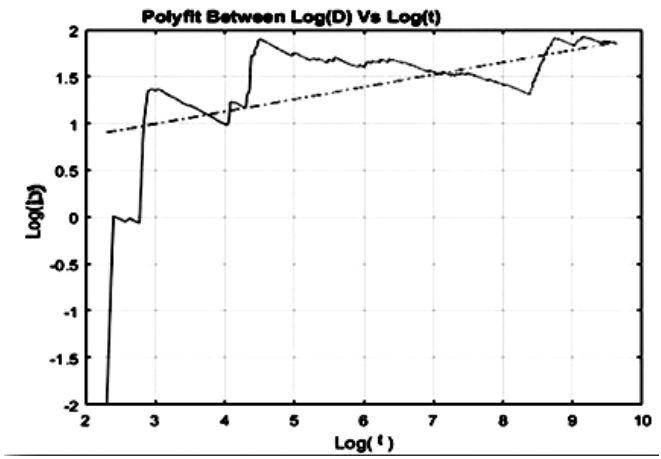

Figure 2

Log (*D*) vs. log (*t*) for Smoothed Solar Flare Index Signal using *FVSM.*

At the next step we have applied Higuchi method on the present smoothed signal taking *k* up to 50 and the calculation gives the value of fractal dimension as 1.644 which confirms the fractal nature of the governing physical process as the present value of *D* lies well within the interval (1, 2). The corresponding graph is given below.

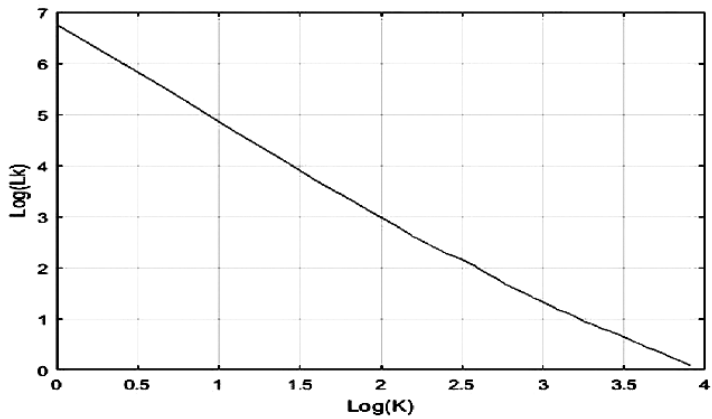

Figure 3

Log (L_k) vs. log (*K*) for Solar Flare Index Signal using Higuchi Method.

Before applying Yule-Walker method we have taken the monthly average of the smoothed signal just to remove irregular fluctuations as these fluctuations can sometimes yield erroneous measurement of autocorrelation coefficients. Next using Yule-walker method in the present monthly average smoothed signal we get the auto correlation functions (*ACF*) at different lags as follows:

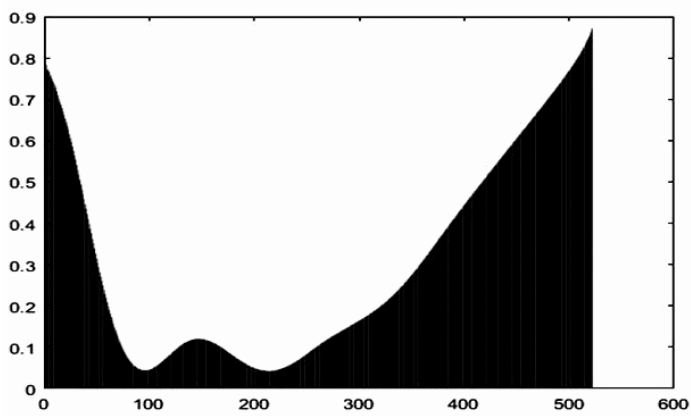

Figure 4
ACF vs. lag for Monthly Average Smoothed Solar Flare Index Signal.

Next we calculate the partial autocorrelation functions (*PACF*) for the same as below:

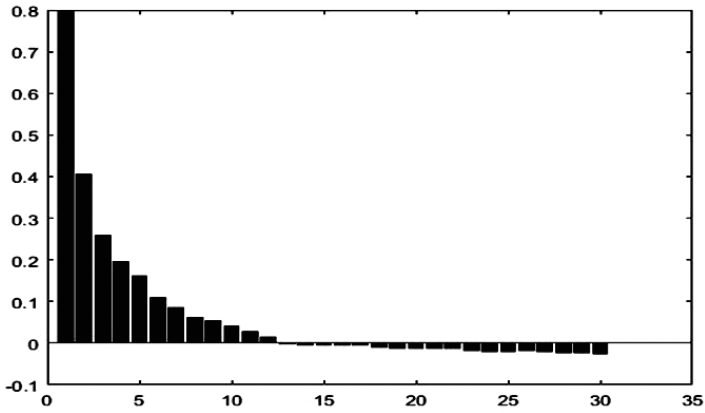

Figure 5
PACF vs. lag for Monthly Average Smoothed Solar Flare Index Signal.

From Figure 5 we can confirm that the present signal is governed by an autoregressive method of order 10 which can be considered as a short order in view of the present size 516 for the monthly average smoothed signal.

4. Conclusion

Here the calculation indicates that the present Solar Flare Index signal follows a short memory process. In this context it must be stated that Rypdal and Rypdal[15] observed the value of Hurst exponent for Solar Flare Index signal as 0.9 using *R/S* method which suggests a strong persistent process. We have also separately calculated the Hurst exponent for the present signal using *R/S* method and calculation leads to a value as H=0.7927 which also refers a long memory process. This may generate a fallacy as for the same signal two existing methods give rise to two mutually separate conclusions. The problem perhaps appears due to the inaccuracy of the *R/S* method as in this method the alterations of average as well as standard deviation are deeply influenced by the changing sizes of the signal. Even the outputs in this method may not portray the behaviour of the entire signal in totality as it always captures the results dynamically for the first halves for the repeated bisections. Probably *R/S* method works well if the corresponding signal possesses homogeneous memory throughout. Here just to verify the homogeneity in the present signal we have employed *FVSM* on the same Solar Flare Index signal taking the reverse order and study gives a result as H=0.47. This possibly indicates that the present signal does not possess any homogeneous memory and that is why the use of *R/S* in the present case may lead to an erroneous result. On the other hand, *FVSM* seems to be more convincing method as it dynamically wraps the entire signal by a cumulative process.

The present study also indicates that the governing process is an autoregressive method of order 10 which confirms its anti-persistence. We have also got an evidence of its self affine nature using Higuchi method. In fine the present study possibly points out that sudden eruption of magnetic energy released on or near the surface of the Sun is a short memory process governed by a self similar as well as autoregressive method.

References

1. IntermittenThe Mysterious Origins of Solar Flares, Scientific American (April, 2006).
2. Brown, R. G. – Exponential Smoothing for Predicting Demand, Cambridge, Arthur. D. Little Inc.,**15** (1956).
3. Holt, C. C. –Forecasting Trends and Seasonal by Exponentially Weighted Averages, Office of Naval Research Memorandum, 52 (1957).
4. Winters, P. R. – Forecasting Sales by Exponentially Weighted Moving Average, Management Science, **6(3),** 324 (1960).
5. Mandelbrot, B.B. – The fractal geometry of nature. W. H. Freeman and Company, New York (1982).
6. Higuchi, T. –Approach to an irregular time series on the basis of the fractal theory, Physica, D **31,** 277 (1988).
7. Higuchi, T. – Relationship between the fractal dimension and the power law index for a time series: a numerical investigation, Physica D: Nonlinear Phenomena, **46(2),** 254 (1990).
8. Hurst, H.E. – Long-term storage capacity of reservoirs, Transactions of American Society of Civil Engineers, **116**, 770 (1951).
9. Scafetta, N. and Grigolini, P. – Scaling detection in signal: diffusion entropy analysis. Physical Review E, **66,** 036130 (2002).
10. Sarkar, A., Barat, P., Mukherjee, P. and Bandyopadhyay, S. K. – Scaling Analysis of Daily Sunspot Numbers, Proceedings of National Conference on Nonlinear Systems and Dynamics (held at A.M.U., Aligarh during February 24-26, 2005), 155 (2005).
11. Yule, G. – On a Method of Investigating Periodicities in Disturbed Series, with Special Reference to Wolfer's Sunspot Numbers, Philosophical Transactions of the Royal Society of London, Ser. A, **226,** 267 (1927).
12. Walker, G. – On Periodicity in Series of Related Terms, Proceedings of the Royal Society of London, Ser., A, **131,** 518 (1931).

13. Box, G.E.P., Jenkins, G.M. and Reinsel, G. C. –Time Series Analysis: Forecasting and Control, Wiley (1976).

14. Patra, S.N., Bhattacharya, G., Ghosh, K. and Raychaudhuri, P.–Search for periodicities of the Solar Irradiance Data from Earth Radiation Budget Satellite (ERBS) using Rayleigh Power Spectrum Analysis, Astrophysics and Space Science, **324 (1),** 47 (2009).

15. Rypdal, M. and Rypdal, K. – Is there long-range memory in solar activity on timescales shorter than the sunspot period? Journal of Geophysical Research, **117,** A04103 (2012).

INFORMATION TO AUTHORS

Manuscripts should represent results of original works on theoretical physics or experimental physics with theoretical background or on applied mathematics. Letters to the Editor and Review articles in emerging areas are also published. Submission of the manuscript will be deemed to imply that it has not been published previously and is not under consideration for publication elsewhere (either partly or wholly) and further that, if accepted, it will not be published elsewhere. It is the right of the Editorial Board to accept or to reject the paper after taking into consideration the opinions of the referees.

Manuscripts may be submitted in pdf/MS word format to **admin@citphy.org or susil_vcsarkar@yahoo.co.in** Online submission of the paper through our **website: www.citphy.org** is also accepted. The file should be prepared with 2.5 cm margin on all sides and a line spacing of 1.5.

The title of the paper should be short and self-explanatory. All the papers must have an abstract of not more than 200 words, the abstract page must not be a part of the main file. Abstract should be self-contained. It should be clear, concise and informative giving the scope of the research and significant results reported in the paper. Below the abstract four to six key words must be provided for indexing and infornjation retrieval.

The main file should be divided into sections (and sub-sections, if necessary) starting preferably with introduction and ending with conclusion. Displayed formula must be clearly typed (with symbols defmed) each on a separate /'ine and well-separated from the adjacent text. Equations should be numbered with on the right-hand side consecutively throughout the text. Figures and Tables with captions should be numbered in Arabic numerals in the order of occurrence in the text and these should be embedded at appropriate places in the text. Associated symbols must invariably follow SI practice.

References should be cited in the text by the Arabic numerals as superscript. All the references to the published papers should be numbered serially by Arabic numerals and given at the end of the paper. Each reference should include the author's name, title, abbreviated name of the journal, volume number, year of publication, page numbers, as in the simple citation given below :

For Periodicals : Sen, N.R. - On decay of energy spectrum of Isotopic Turbulence, 1. Appl. Phys. **28,** No. l0, l09-110 (1999).

1. Mikhilin, S. G. - Integral Equations, Pergamon Press, New York (1964).
2. Hinze, A. K. - Turbulence Study of Distributed Turbulent Boundary Layer Flow, Ph.D, Thesis, Rorke University (1970).

The corresponding author will receive page proof, typically as a pdf file. The proof should be checked carefully and returned to the editorial office within two or three days. Corrections to the proof should be restricted to printing errors and made according to standard practice. At this stage any modifications (if any) made in the text should be highlighted.

To support the cost of publication of the journal, the authors (or their Institutions) are requested to pay publication charge Rs.200/- per printed page for authors of Indian Institutes and US$ 20 for others. Publication charges to be sent directly to **CALCUTTA INSTITUTE OF THEORETICAL PHYSICS, 'BIGNAN KUTIR', 4/1, MOHAN BAGAN LANE, KOLKATA-700 004, INDIA.**

A pdf of the final publisher's version of the paper will be sent to the corresponding author shortly after print publication by our Co-publisher, **Wilcox Books & Periodicals Co. (wilcoxbooks@gmail.com)**

All communications are to be sent to the Secretary, Calcutta Institute of Theoretical Physics, 'Bignan Kutir', 4/1, Mohan Bagan Lane, Kolkata-700 004.

Indian Journal of Theoretical Physics is in the list of Journals approved by UGC.

For details please visit our website www.citphy.org

PUBLICATIONS
OF
CALCUTTA INSTITUTE OF THEORETICAL PHYSICS
"BIGNAN KUTIR"
4/1, Mohan Bagan Lane, Kolkata-700 004, India
Phone : +91-33-25555726

INDIAN JOURNAL OF THEORETICAL PHYSICS (ISSN : 0019-5693)
Research Journal containing Original Papers, Review Articles and Letters to the Editor is published quarterly in March, June, September and December and circulated all over the world.

Subscription Rates
₹ 1500 per volume (for Bonafide Indian Party)
US$ 350 (for Foreign Party)

Back Volume Rates
₹ 1500 per volume (for Bonafide Indian Party)
US$ 350 per volume or Equivalent Pounds per volume

Books Written by Prof. K. C. Kar, D. Sc.

- **INTRODUCTION TO THEORETICAL PHYSICS [Vol. I and Vol. II (Acoustics)]** Useful to students of higher physics
  Price :₹ 60 or US $ 10 per volume
- **WAVE STATISTICS : Its principles and Applications [Vol. I and Vol. II]** Useful to Post Graduate and Research students
  Price :₹ 80 or US $ 12
- **STATISTICAL MECHANICS : PRINCIPLES AND APPLICATIONS [Vol. I and Vol. II]** Useful to Advanced students of theoretical Physics
  Price :₹ 120 or US $ 15
- **A NEW APPROACH TO THE THEORY OFRELATIVITY [Vol. I and Vol. II]** Useful to Post Graduate and advanced students
  Price :₹ 50 or US $ 8

Order may be sent directly to Calcutta Institute of Theoretical Physics
"BignanKutir", 4/1, Mohan Bagan Lane, Kolkata-700 004, India